The generation of axial vorticity in solid-propellant rocket-motor flows.

By S. BALACHANDAR[1], J. D. BUCKMASTER[2,1] and M. SHORT[1]

[1]Theoretical and Applied Mechanics, University of Illinois, Urbana, IL 61801, USA.
[2]Aeronautical and Astronautical Engineering, University of Illinois, Urbana, IL 61801, USA.

(Received April 1999)

We examine small deviations from axial symmetry in a solid-propellant rocket motor, and describe a 'bath-tub-vortex' effect, in which substantial axial vorticity is generated in a neighborhood of the chamber center-line. The unperturbed flow field is essentially inviscid at modest Reynolds numbers, even at the chamber walls, as has long been known, but the inviscid perturbed flow is singular at the center-line, and viscous terms are required to regularize it. We examine perturbations sufficiently small that a linear analysis is valid everywhere (εRe small, where ε is a measure of the perturbation amplitude and Re is a Reynolds number); and larger perturbations in which a nonlinear patch is created near the center-line of radius $O(\sqrt{\varepsilon})$. Our results provide an explanation of swirl experimentally observed by others, and a cautionary note for those concerned with numerical simulations of these flows, whether laminar or turbulent.

1. Introduction

It has been known since the pioneering work of Taylor (1956) that interior flows generated by a flux at the boundary can (indeed must) satisfy the no-slip condition without benefit of viscosity, since the boundary layer is blown off by the injection. An important example is the flow inside a solid-propellant rocket motor, a problem that was first discussed by Culick (1966): he constructed an inviscid rotational solution for flow in a long right-circular cylinder with side-wall injection. Curiously, there has been little if any work on flows in channels with more complex cross-sections, despite the fact that solid propellant grain configurations are seldom circular (Sutton 1992), and it is this issue that is the subject of the present paper. More precisely, we are concerned with flows that are not axisymmetric, either because the cross-section is not axisymmetric, or because of variations in the injection (burning) rate around the circumference.

The general problem is not amenable to analysis, and we do not consider it here: instead, we consider perturbations of Culick's solution. We find that viscous terms can not be neglected everywhere, although there is no boundary layer, and a linear analysis is only valid if $\varepsilon Re << 1$, where ε is a measure of the perturbation and Re is an appropriate Reynolds number. Otherwise a nonlinear axial patch of radius $\sim \sqrt{\varepsilon}$ exists in which the axial vorticity is $O(1)$. This vorticity is an increasing function of Re, with magnitude $\sim Re$ when $\varepsilon Re >> 1$. Our general conclusion is that modest deviations from symmetry can have profound effects on the nature of the flow-field.

Our analysis process is as follows. We show why there can be no side-wall boundary layer in a long cylinder with side-wall injection; we formulate the equations for a large aspect-ratio cylinder; and we identify Culick's solution for a circular cross-section. We then consider small inviscid perturbations to Culick's solution and show that the axial vorticity, a perturbation quantity, is singular like $1/r^2$ as $r \to 0$. This solution can be regularized by viscous terms, important on the scale $r = O(1/\sqrt{Re})$, and in this ***viscous core*** the axial vorticity is $O(\varepsilon Re)$, which must be small. A complete description of the perturbation flow field is presented, both within the viscous core and in the surrounding inviscid annulus. When εRe is not small it is shown that there is a nonlinear patch on the scale $r = O(\sqrt{\varepsilon})$ embedded in the linearly perturbed inviscid flow, and that in this patch the axial vorticity is $O(1)$. Again, viscous terms are needed within a viscous core to regularize the solution as $r \to 0$, and because of this the vorticity is an unbounded function of Re. Solutions within the nonlinear patch are constructed numerically.

2. Rocket-chamber flows and blow-off of the boundary layer

A solid-propellant rocket-motor consists of a chamber, lined with propellant, to which a nozzle is attached. Combustion processes in the neighborhood of the propellant surface heat the propellant, causing it to regress, and generating voluminous quantities of gas. Because of the disparity between the gas density and the solid density, the gas velocity normal to the surface is much greater than the regression rate, so that on gas-phase time scales the flow may be modelled by flow injection from a fixed surface. That this surface can not support a boundary-layer is apparent from the following argument.

Consider the rocket chamber shown in Fig. 1 which, for the purposes of the immediate argument, we will suppose is two-dimensional (plane). We seek a description of the flow-field in terms of the classical dichotomy of an inviscid irrotational core flow and Prandtl boundary layers. The core-flow is

$$(v, w) = \frac{2v_n}{D}\left(-y + \frac{D}{2}, z\right) \tag{2.1}$$

where v_n is the wall normal injection velocity and D is the separation distance between the top and bottom walls. Then the speed at the edge of the boundary-layer on the lower wall is

$$w(z) = \frac{2v_n z}{D}, \tag{2.2}$$

as in Hiemenz flow. Unlike the classical Hiemenz configuration, however, there is a substantial blowing velocity and the boundary conditions at the wall are

$$(v, w) = (v_n, 0) \text{ at } y = 0. \tag{2.3}$$

A boundary layer solution, if it existed, would be valid for values of $z \gg D$, a region well removed from end-wall effects.

The inviscid solution (2.1) is characterized by a rate of strain

$$\alpha = \frac{2v_n}{D} \tag{2.4}$$

from which a characteristic speed $\sqrt{\alpha\nu}$ can be defined, a measure of v in the Hiemenz solution. Thus for a boundary layer solution to exist, necessarily

$$v_n \leq \sqrt{\alpha\nu}, \text{ i.e. } v_n \leq \frac{2\nu}{D}. \tag{2.5}$$

With $\nu = 1.6\times10^{-2} ft^3/s$, a value appropriate for a temperature of $3000K$, and $D = 2ft$, then $2\nu/D \sim 5mm/s$ which is much smaller than a typical blowing velocity, as the regression rate of the *solid* is $\sim$ 1cm/s. But the difficulty is not merely one identified from quantitative considerations. For the length $(\nu/\alpha)^{1/2}$ is characteristic of the boundary layer thickness, so that we require

$$\sqrt{\frac{\nu}{\alpha}} \ll \frac{D}{2}, \quad \text{i.e.} \quad v_n \gg \frac{2\nu}{D}, \tag{2.6}$$

in contradistinction with the inequality (2.5). Thus blow-off is assured.

3. Inviscid flow in a large aspect-ratio chamber

In the absence of a boundary layer we seek rotational solutions of Eulers equations that satisfy the no-slip condition at the wall in addition to the blowing condition. Note that there is no difficulty in prescribing the values of all three velocity components at the wall where the characteristics (streamlines) enter the domain. Only if the flow were potential would this not be possible, equivalent to the simultaneous specification of Dirichlet and Neumann data for a harmonic function.

Figure 1 is still appropriate, but now cylindrical with arbitrary cross-section. Also we place the origin of the co-ordinate system on some appropriately chosen axis, rather than at the side-wall. We have

$$\nabla \cdot \mathbf{q} = 0, \quad \mathbf{q} \cdot \nabla \mathbf{q} = -\frac{1}{\rho}\nabla p, \quad \mathbf{q} = (u, v, w). \tag{3.1}$$

The variables are now scaled in the following fashion: u and v with v_n; w with $2v_nL/D$; x and y with $D/2$; z with L; p with $4\rho v_n^2 L^2/D^2$. Moreover we write the scaled pressure as

$$\bar{p} = P_0(z) + \frac{D^2}{4L^2}P_1 \tag{3.2}$$

and assume that $D/L \ll 1$, whence

$$\bar{\nabla} \cdot \bar{\mathbf{q}} = 0, \quad \bar{\mathbf{q}} \cdot \bar{\nabla}\begin{pmatrix} \bar{u} \\ \bar{v} \end{pmatrix} = \begin{pmatrix} -\partial P_1/\partial \bar{x} \\ -\partial P_1/\partial \bar{y} \end{pmatrix}, \quad \bar{\mathbf{q}} \cdot \bar{\nabla}\bar{w} = -\frac{dP_0}{dz}. \tag{3.3}$$

These equations have a separable solution of the form:

$$\bar{w} = z\tilde{w}(\bar{x}, \bar{y}), \ \bar{u} = \tilde{u}(\bar{x}, \bar{y}), \ \bar{v} = \tilde{v}(\bar{x}, \bar{y}), \ P_0 = -\frac{1}{2}Cz^2, \ P_1 \equiv P_1(\bar{x}, \bar{y}), \tag{3.4}$$

with C a constant, whereupon (3.3) reduce to

$$\begin{aligned} \frac{\partial \tilde{u}}{\partial \bar{x}} + \frac{\partial \tilde{v}}{\partial \bar{y}} + \tilde{w} &= 0, \\ \tilde{u}\frac{\partial \tilde{w}}{\partial \bar{x}} + \tilde{v}\frac{\partial \tilde{w}}{\partial \bar{y}} + \tilde{w}^2 &= C, \\ \left(\tilde{u}\frac{\partial}{\partial \bar{x}} + \tilde{v}\frac{\partial}{\partial \bar{y}}\right)\begin{pmatrix} \tilde{u} \\ \tilde{v} \end{pmatrix} &= \begin{pmatrix} -\partial P_1/\partial \bar{x} \\ -\partial P_1/\partial \bar{y} \end{pmatrix}. \end{aligned} \tag{3.5}$$

These equations describe the flow field for a large aspect-ratio chamber when $z \gg D$. The boundary conditions on the chamber walls are:

$$\tilde{w} = 0, \quad (\tilde{u}, \tilde{v}) \cdot \mathbf{n} = 1, \quad (\tilde{u}, \tilde{v}) \times \mathbf{n} = 0, \tag{3.6}$$

where $\mathbf{n}$ is the inner normal.

The solution for a circular cylinder of unit radius, first given by Culick (1966), is

$$\tilde{v}_r = -\frac{1}{\bar{r}}\sin\left(\frac{\pi}{2}\bar{r}^2\right), \quad \tilde{w} = \pi\cos\left(\frac{\pi}{2}\bar{r}^2\right), \quad C = \pi^2. \tag{3.7}$$

It is not difficult to show that the axisymmetric equations reduce to the plane equations under the substitutions $\bar{r}\tilde{v}_r \to \tilde{v}, \bar{r}^2 \to \bar{y}, \tilde{w} \to 2\tilde{w}, C \to 4C$, whence the solution in the plane case is

$$\tilde{v} = -\sin\left(\frac{\pi}{2}\bar{y}\right), \quad \tilde{w} = \frac{\pi}{2}\cos\left(\frac{\pi}{2}\bar{y}\right), \quad C = \frac{1}{4}\pi^2. \tag{3.8}$$

4. Finite Reynolds Number Solutions

The viscous counterparts to (3.5)b,c,d are

$$\begin{gathered} \tilde{u}\frac{\partial \tilde{w}}{\partial \bar{x}} + \tilde{v}\frac{\partial \tilde{w}}{\partial \bar{y}} + \tilde{w}^2 = C + \frac{1}{Re}\nabla_c^2 \tilde{w}, \\ \left(\tilde{u}\frac{\partial}{\partial \bar{x}} + \tilde{v}\frac{\partial}{\partial \bar{y}}\right)\begin{pmatrix}\tilde{u}\\ \tilde{v}\end{pmatrix} = \begin{pmatrix}-\partial P_1/\partial \bar{x} + \nabla_c^2 \tilde{u} \\ -\partial P_1/\partial \bar{y} + \nabla_c^2 \tilde{v}\end{pmatrix}, \\ \nabla_c^2 \equiv \frac{\partial^2}{\partial \bar{x}^2} + \frac{\partial^2}{\partial \bar{y}^2}, \end{gathered} \tag{4.1}$$

where $Re = v_n D/2\nu$. (3.5)a and the boundary conditions (3.6) are unchanged. Numerical solution leads not only to a description of the velocity field, but also to a description of the manner in which the pressure gradient C varies with Re, Fig.2. Note that the large Re values are consistent with (3.7)c, (3.8)c. The small Reynolds number behavior is

$$\begin{aligned} C &= \frac{16}{Re} + 12 + O(Re) \text{ (axisymmetric)}, \\ C &= \frac{3}{Re} + \frac{81}{35} + O(Re) \text{ (plane)}, \end{aligned} \tag{4.2}$$

with corresponding velocity fields

$$\begin{aligned} \tilde{v}_r &= (\bar{r}^3 - 2\bar{r}), \ \tilde{w} = 4(1-\bar{r}^2) \ \text{(axisymmetric)}, \\ \tilde{v} &= \frac{1}{2}(\bar{y}^3 - 3\bar{y}), \ \tilde{w} = \frac{3}{2}(1-\bar{y}^2) \ \text{(plane)}. \end{aligned} \tag{4.3}$$

Results intermediate between the limiting results (3.7), (3.8), (4.2) and (4.3) are shown in Figs. 3 and 4, from which it is clear that the inviscid limit provides an accurate approximation for $Re > 100$.

5. Perturbations of the circular-cylinder flow (linear analysis)

Consider a chamber whose cross-section is defined by

$$\bar{r} = 1 + \varepsilon R(\theta), \ \varepsilon << 1. \tag{5.1}$$

We shall construct perturbations to the solution (3.7), generated in this way. Our analysis is also capable of accounting for perturbations generated in other ways, for example by variations in the injection speed v_n. Consider (3.5) and (3.6) dropping $\tilde{}$ and $\bar{}$. We seek solutions

$$w = w_0 + \varepsilon w_1, \ v_r = v_{r_0} + \varepsilon v_{r_1}, \ v_\theta = \varepsilon v_{\theta_1}, \ P_1 = p_0 + \varepsilon p_1, \ \Omega = \varepsilon \Omega_1, \tag{5.2}$$

where Ω is the magnitude of the axial vorticity and v_{r_0}, w_0 is the solution (3.7). Since the axial vorticity transport equation is

$$(\hat{\mathbf{q}} \cdot \nabla)\Omega - w\Omega = 0, \ \hat{\mathbf{q}} = (u, v, 0), \tag{5.3}$$

Ω_1 satisfies the equation

$$\frac{1}{\Omega_1}\frac{\partial\Omega_1}{\partial r} = -\pi r \cot\left(\frac{\pi}{2}r^2\right), \tag{5.4}$$

whence

$$\Omega_1 \sin\frac{\pi}{2}r^2 = \text{const.} \tag{5.5}$$

It is tempting to eliminate the singular behavior at $r = 0$ by setting the constant equal to 0 so that the perturbation cross-flow is a potential flow (albeit not harmonic, since it is not solenoidal). But in general such a flow can not simultaneously satisfy the boundary conditions (3.6), and this deficiency can not be accomodated by placing a boundary layer at the wall. To regularize the solution, viscous terms must be retained and (4.1) must be considered. The viscous terms are important on the scale $r = O\left(1/\sqrt{Re}\right)$ where $\Omega_1 = O(Re)$ so that the axial vorticity Ω is $O(\epsilon Re)$. Thus the perturbations are only small everywhere if εRe is small. Later we shall relax this restriction, meantime noting that the linear analysis of this section is relevant to the larger context.

6. Solution of the vorticity equation

When $Re \gg 1$ the inviscid solution (5.5) is correct provided $r \gg 1/\sqrt{Re}$. Otherwise, Ω_1 satisfies the equation

$$-\frac{1}{r}\sin\left(\frac{\pi}{2}r^2\right)\frac{\partial\Omega_1}{\partial r} = \pi\cos\left(\frac{\pi}{2}r^2\right)\Omega_1 + \frac{1}{Re}\nabla^2\Omega_1 \tag{6.1}$$

which, in the viscous core $r = O\left(1/\sqrt{Re}\right)$, can be approximated by

$$-\frac{\pi s}{2}\frac{\partial\Omega_1}{\partial s} = \pi\Omega_1 + \frac{\partial^2\Omega_1}{\partial s^2} + \frac{1}{s}\frac{\partial\Omega_1}{\partial s} - \frac{n^2}{s^2}\Omega_1, \tag{6.2}$$

where $s = r\sqrt{Re}$ and we have assumed an angular dependence $e^{in\theta}$ for some non-vanishing positive integer n. (The special and simple case $n = 0$ is discussed later). Because the perturbations that we consider are of this nature, there are no perturbations to the constant C of (3.5)b.

Solutions of (6.2) behave like $s^{\pm n}$ as $s \to 0$, and we define $H_n(s)$ to be the solution that satisfies the condition

$$\lim_{s\to 0} H_n s^{-n} = 1. \tag{6.3}$$

Also, H_n must behave like $1/s^2$ as $s \to \infty$ in order to match with the inviscid solution (5.5). The required solution is

$$H_n(s) = \frac{s^n \int_{-1/4}^{0} dp e^{\pi p s^2}(-p)^{n/2}(1+4p)^{n/2-1}}{\int_{-1/4}^{0} dp(-p)^{n/2}(1+4p)^{n/2-1}}, \tag{6.4}$$

which can be evaluated in terms of elementary functions when n is an even integer.

For large values of s,

$$H_n \sim \frac{\pi^{-1-n/2}\int_{-\infty}^{0} dp e^{p}(-p)^{n/2}}{s^2\int_{-1/4}^{0} dp(-p)^{n/2}(1+4p)^{n/2-1}} \equiv \frac{a}{s^2}. \tag{6.5}$$

Then if we write

$$\Omega_1 = A\,\text{cosec}\left(\frac{\pi}{2}r^2\right)e^{in\theta} \tag{6.6}$$

in the inviscid annulus (cf. (5.5)).

$$\Omega_1 = \frac{2ARe}{a\pi} H_n(s) e^{in\theta} \tag{6.7}$$

in the viscous core. These formulas provide a description of Ω_1 everywhere to within a constant (A). Graphs of $H_n(s)/a$ are shown in Fig. 5 for various values of n.

7. The velocity field

The following estimates are valid within the viscous core:

$$u_1, v_1 = O\left(\sqrt{Re}\right), \; w_1 = O\left(\frac{1}{Re}\right), \; \Omega_1 = O(Re). \tag{7.1}$$

Then, to leading order within the core,

$$\frac{\partial u_1}{\partial y} - \frac{\partial v_1}{\partial x} = \Omega_1, \; \frac{\partial u_1}{\partial x} + \frac{\partial v_1}{\partial y} = 0, \tag{7.2}$$

so that a stream function may be defined ($u_1 = \partial\psi/\partial y, \; v_1 = -\partial\psi/\partial x$) and

$$\frac{\partial^2 \psi}{\partial s^2} + \frac{1}{s}\frac{\partial \psi}{\partial s} - \frac{n^2}{s^2}\psi = \frac{2AH_n(s)}{a\pi} e^{in\theta} \equiv f. \tag{7.3}$$

The solution that is regular at the origin is

$$\psi = C_1 s^n e^{in\vartheta} + \frac{s^n}{2n}\int_0^s ds f s^{-n+1} - \frac{s^{-n}}{2n}\int_0^s ds f s^{n+1} \tag{7.4}$$

and we must choose $C_1 = -\frac{1}{2n}\int_0^\infty ds e^{-in\theta} f s^{-n+1}$ so that

$$\psi \sim \frac{-2Ae^{in\vartheta}}{\pi n^2}, \; v_{r_1} \sim \frac{-2iA\sqrt{Re_D} e^{in\theta}}{\pi n s} \text{ as } s \to \infty. \tag{7.5}$$

In the inviscid annulus v_{r_1} is singular like $1/r$, consistent with the $1/r^2$ singularity in Ω_1, and this behavior matches (7.5)b. We now turn to the solution in the inviscid annulus.

8. The inviscid annulus, $\frac{1}{\sqrt{Re}} \ll r \leq 1$

Consider continuity, (3.5)a, and the definition of Ω: These can be used to express v_{θ_1} and v_{r_1} in terms of Ω_1 and w_1. Thus

$$\frac{in}{r} v_{r_1} = \Omega_1 + \frac{\partial v_{\theta_1}}{\partial r} + \frac{1}{r} v_{\theta_1}, \tag{8.1}$$

and

$$v_{\theta_1} = r^{-1+n}\left[C_2 + \frac{1}{2n}\int_1^r dr\, r^{2-n} g\right] + r^{-1-n}\left[v_{\theta_1}(1) - C_2 - \frac{1}{2n}\int_1^r dr\, r^{2+n} g\right] \tag{8.2}$$

where

$$g \equiv \frac{-inw_1}{r} - \frac{1}{r^2}\frac{\partial}{\partial r}(r^2 \Omega_1) \tag{8.3}$$

and C_2 is determined by evaluating (8.1) at $r = 1$, whence

$$0 = inv_{r_1}(1) + nv_{\theta_1}(1) - A - 2nC_2. \tag{8.4}$$

In addition, the perturbed z – momentum equation, when solved for w_1, yields

$$w_1 = \sin^2\left(\frac{\pi r^2}{2}\right)\left[w_1(1) - \int_1^r \frac{dr_1 v_{r_1}\pi^2 r^2}{\sin^2(\pi r^2/2)}\right], \tag{8.5}$$

from which we conclude that w_1 vanishes like r^2 as $r \to 0$ (cf. (7.1)b). Thus g vanishes like r as $r \to 0$, and with this information we can examine the small r behavior of v_{θ_1} from (8.2). Unacceptable singular behavior (r^{-1-n}) can only be eliminated if

$$v_{\theta_1}(1) - C_2 - \frac{1}{2n}\int_1^0 dr\, r^{2+n} g = 0 \tag{8.6}$$

and this closes the problem and permits the evaluation of A, the vorticity amplitude (cf. (6.6)).

Solutions can be constructed in the following fashion: We guess w_1 and use Eqns (6.6), (8.4), (8.6) to calculate the constant A: v_{θ_1} is then determined from Eqn (8.2), followed by v_{r_1} from (8.1); and then a new estimate for w_1 follows from (8.5).

Boundary values at $r = 1$ must be assigned, and there are various possibilities. If the cross-section is unperturbed but the injection velocity is

$$v_n = 1 - \varepsilon e^{in\theta} \tag{8.7}$$

then

$$v_{r_1}(1) = e^{in\theta},\ v_{\theta_1}(1) = 0,\ w_1(1) = 0. \tag{8.8}$$

If the injection velocity is fixed but the cross-section is perturbed, viz.

$$r = 1 - \varepsilon e^{in\theta}, \tag{8.9}$$

a shift in the boundary conditions (3.6) to $r = 1$ is equivalent to

$$v_{r_1}(1) = e^{in\theta},\ v_{\theta_1}(1) = 0,\ w_1(1) = -\pi^2 e^{in\theta}. \tag{8.10}$$

In this case the lowest-order relevant mode corresponds to $n = 2$, as the case $n = 1$ is equivalent to mere displacement of the circular boundary without substantive effect on the flow field. Solutions for both these cases are shown in Figs. 6,7.

9. Numerical solution of the linear problem

In addition to the asymptotic treatment, we have calculated the small perturbation solutions by numerically solving the linearized equations for finite Reynolds numbers. Care is required in guaranteeing proper behavior of the solution in the neighborhood of the origin. For the velocity components to be analytic there, we require, as $r \to 0$,

$$v_{r1} \to \begin{cases} b_o r & \text{for } n = 0 \\ b_n r^{n-1} & \text{for } n \neq 0 \end{cases}$$
$$v_{\theta 1} \to \begin{cases} c_o r & \text{for } n = 0 \\ ib_n r^{n-1} & \text{for } n \neq 0 \end{cases}$$
$$w_1 \to d_n r^n \text{ for all } n, \tag{9.1}$$

for certain constants b_j, c_j, d_j. This behavior is consistent with the vorticity vanishing as r^n.

Figures 8-10 show the vorticity and velocity perturbations generated by the injection perturbation (8.7) for $n = 1, 2, 3$, and several values of Re. The asymptotic conclusions v_{r_1}, $v_{\theta_1} = O(\sqrt{Re})$, $w_1 = O(1/Re)$, $\Omega_1 = O(Re)$ within the viscous core of diameter

$O(1/\sqrt{Re})$ are well evident in these figures. The radial velocity shows $1/r$ behavior and the axial vorticity shows $1/r^2$ behavior within the inviscid annulus, singular behavior as the origin is approached that is regularized within the viscous core. The *intensity* of the viscous core, measured both by the magnitude of the perturbations within it and its narrowness, decreases with increasing mode number. Note that $v_{\theta 1}$ and v_{r1} do not vanish at $r=0$ when $n=1$, but do vanish there when $n \neq 1$.

Figures 11 & 12 show the corresponding results for $n=2$ and $n=3$ when the cross-section is perturbed with the injection velocity fixed, (8.9).

9.1. *The case* $n = 0$

Here an exact solution can be constructed without approximation, since v_θ and Ω satisfy the equations

$$v_{r0}\frac{\partial \Omega}{\partial r} - w_0\Omega = \frac{1}{Re}\frac{1}{r^2}\frac{\partial}{\partial r}(r\frac{\partial \Omega}{\partial r}), \qquad (9.2)$$
$$\Omega = -\frac{1}{r}\frac{\partial}{\partial r}(rv_\theta),$$

Thus

$$\frac{\Omega}{\Omega(0)} = \exp\left[-Re\int_0^r \frac{dr}{r}\sin\left(\frac{\pi}{2}r^2\right)\right] = \exp\left[-\frac{Re}{2}\mathrm{Si}\left(\frac{\pi}{2}r^2\right)\right], \qquad (9.3)$$

(see Fig.13a) which behaves like

$$\exp\left(-\frac{\pi}{4}s^2\right) \equiv H_0(s) \qquad (9.4)$$

in the viscous core when Re is large, and is exponentially small in the inviscid annulus. Here $\mathrm{Si}(x)$ is the Sine Integral. v_θ is obtained by quadrature, Fig.13b, and for large Re has the uniformly valid representation

$$\frac{Re}{\Omega(0)}v_\theta \sim -\frac{2}{\pi}\frac{\sqrt{Re}}{s}\left[1 - e^{-\pi s^2/4}\right] \qquad (9.5)$$

which behaves like $-2/\pi r$ in the inviscid annulus.

10. Solution when $\varepsilon \ll 1$ and $\varepsilon \gg 1/Re$ *or* $\varepsilon = O(1/Re)$

The linear analysis ($n \neq 0$) of the previous sections is of little if any practical interest when applied everywhere in the chamber, since the perturbations are necessarily very small for realistic values of the Reynolds number. And so in this section we consider larger perturbations for which part of the perturbation flow-field is nonlinear. With the earlier analysis this constitutes a complete description when $\varepsilon \ll 1$, for any value of Re.

Our starting point is the small r behavior:

$$\Omega \sim \frac{\varepsilon 2Ae^{in\theta}}{\pi r^2} \quad \text{(see (6.6))}; \qquad (10.1)$$

$$\varepsilon v_{r_1} \sim \frac{-\varepsilon i2Ae^{in\theta}}{n\pi r} \qquad (10.2)$$

(from (8.1), noting that v_{θ_1} vanishes at least as rapidly as r);

$$v_{r_0} \sim -\frac{\pi}{2}r, \; w \sim \pi. \qquad (10.3)$$

From these it is apparent that v_{r_0} and εv_{r_1} are comparable when $r = O(\sqrt{\varepsilon})$. On this scale there is a nonlinear description in which

$$\Omega, w = O(1); \quad v_r,\ v_\theta = O(\sqrt{\varepsilon}). \tag{10.4}$$

We shall call this region the *nonlinear patch.* When $\varepsilon Re = O(1)$, viscous terms are important on the same scale; when $\varepsilon Re \gg 1$, viscous terms are only important on a smaller scale, defining a viscous core.

In the scaled variables appropriate for the nonlinear patch ($r = \sqrt{\varepsilon} r^+$, **etc.**) we have

$$\begin{aligned}
\Omega^+ &= \frac{1}{r^+}\frac{\partial v_r^+}{\partial\theta} - \frac{1}{r^+}\frac{\partial}{\partial r^+}(r^+ v_\theta^+),\\
u^+\frac{\partial w^+}{\partial x^+} &+ v^+\frac{\partial w^+}{\partial y^+} + w^{+2} = \pi^2,\\
\frac{1}{r^+}\frac{\partial}{\partial r^+}\left(r^+ v_r^+\right) &+ \frac{1}{r^+}\frac{\partial v_\theta^+}{\partial\theta} + w^+ = 0,\\
v_r^+\frac{\partial\Omega^+}{\partial r^+} + \frac{v_\theta^+}{r^+}\frac{\partial\Omega^+}{\partial\theta} &= w^+\Omega^+ + \frac{1}{\varepsilon Re}\nabla^{+2}\Omega^+.
\end{aligned} \tag{10.5}$$

The appropriate solution of (10.5)b is

$$w^+ = \pi. \tag{10.6}$$

Then, writing

$$v_r^+ = -\frac{\pi}{2}r^+ + V_r^+, \tag{10.7}$$

continuity, (10.5)c, becomes

$$\frac{1}{r^+}\frac{\partial}{\partial r^+}\left(r^+ V_r^+\right) + \frac{1}{r^+}\frac{\partial v_\theta^+}{\partial\theta} = 0 \tag{10.8}$$

which can be satisfied by the introduction of the stream function Ψ^+, viz.

$$V_r^+ = \frac{1}{r^+}\frac{\partial\Psi^+}{\partial\theta}, \quad v_\theta^+ = -\frac{\partial\Psi^+}{\partial r^+}, \tag{10.9}$$

whence

$$\Omega^+ = \nabla^{+2}\Psi^+. \tag{10.10}$$

The vorticity transport equation becomes

$$\left(-\frac{\pi}{2}r^+ + \frac{1}{r^+}\frac{\partial\Psi^+}{\partial\theta}\right)\frac{\partial\Omega^+}{\partial r^+} - \frac{1}{r^+}\frac{\partial\Psi^+}{\partial r^+}\frac{\partial\Omega^+}{\partial\theta} = \pi\Omega^+ + \frac{1}{\varepsilon Re}\nabla^{+2}\Omega^+. \tag{10.11}$$

Matching conditions as $r^+ \to \infty$ are defined by (10.2), (10.3). More precisely, any linear perturbation in the core can be expressed as a Fourier sum of terms of this kind. We shall restrict attention to a single mode, with

$$\Psi^+ \to \frac{-2}{n^2\pi}\cos(n\theta), \quad \Omega^+ \sim \frac{2}{\pi r^{+2}}\cos(n\theta) \text{ as } r^+ \to \infty, \tag{10.12}$$

corresponding to the small r linear description

$$v_r \sim \frac{-\pi}{2}r + \frac{\varepsilon 2}{n\pi r}\sin(n\theta), \quad \Omega \sim \frac{\varepsilon 2\cos(n\theta)}{\pi r^2}. \tag{10.13}$$

We have chosen $A = 1$ (wlog.) since it can be absorbed into ε.

(10.11) is solved numerically, subject to the boundary conditions (10.12), using spectral methods for various values of εRe and n. A Fourier Galerkin scheme is used along the circumferential direction and Chebyshev collocation is used along the radial direction.

With increasing εRe, the effect of nonlinearity increases and correspondingly the resolution requirement also increases. The results to be presented below are obtained using a 21 mode expansion along the circumferential direction, and 51 points along the radial direction. This resolution was found to be adequate over the range of εRe considered here.

Figure 14 shows contours of vorticity and streamfunction plotted for the case $n = 1$ and εRe=1. The outer boundary is chosen to be at $r^+ = 4$. The vorticity exhibits a dipole-like pattern with a peak vorticity magnitude of approximately 0.416 at $r \approx 0.92$. As εRe increases, the vorticity maximum increases (see Fig 15 for $\varepsilon Re = 10$) and the top-bottom symmetry of the pattern is further destroyed. At small εRe the vorticity peaks are separated by 180 degrees. With increasing nonlinearity, the phase relation of the higher circumferential harmonics is such that the angular separation of the points of peak vorticity decreases. The radial location of peak vorticity draws closer to the origin.

Figure 16 shows the vorticity and streamfunction contours for the case $n = 2$, $\varepsilon Re = 1$. The vorticity distribution exhibits a quadrapole pattern with the peak vorticity substantially less than that for $n = 1$. Fig 14. With increasing εRe (see Fig 17 for $\varepsilon Re = 25$) the pattern is distorted and the peak vorticity occurs closer to the origin. Figure 18,19 show the solutions for $n = 3$ and $n = 4$, revealing sextapole and octapole patterns. The maximum vorticity progressively decreases with n, and the symmetry is destroyed with increasing Reynolds number. Figure 20 shows near-origin views of the velocity vector plot (V_r^+, v_θ^+) for the four cases $n = 1, 2, 3, 4$, at $\varepsilon Re = 25$.

The scaling of maximum vorticity with Reynolds number is shown in Fig 21. A near linear scaling of the form $\Omega^+_{peak} = c\varepsilon Re$ is observed with the coefficient c taking values 0.424, 0.147, 0.074, and 0.043 when $n = 1, 2, 3, 4$. The radial location of the vorticity peak is shown in Fig 22a. With increasing εRe the axial vortices first move rapidly towards the origin, but then move away. This behavior can be seen in the $n = 1, 2$ cases and is probably a feature of the solutions for larger n at sufficiently large Reynolds numbers. Finally we quantify the distortion from the regular pole patterns in terms of the smallest angular separation between two adjacent vorticity peaks (see Fig.22b). For vanishing Reynolds number, the separation is $180/n$ degrees. The effect of the nonlinearity is significant for $n = 1, 2$ at the Reynolds numbers we have considered.

11. Concluding Remarks

Our main conclusions can be summarized succintly: Small deviations from axial symmetry in a solid propellant rocket motor flow lead to large values of axial vorticity, and to failure of the inviscid solution near the center-line. Our results make clear that, in numerical simulations, mesh points must be concentrated in a neighborhood of the center-line, and this will be true not only for the laminar flows that we have considered, but also for large eddy simulations of turbulent flows, a subject of great interest at the present time. The mechanisms that are responsible for this are straightforward, analogous to those that create a bath-tub vortex, but do not appear to have been considered before.

Experimental manifestation of swirl generation, albeit unexplained, is reported in Dunlap *et al.* (1990). In the cold-flow simulations of that study, a significant circumferential velocity field was observed, although the chamber was nominally symmetric. This is indicated schematically (Fig.6, loc.cit.) as a simple swirling flow ($n = 0$), but the velocity was only measured in a single longitudinal plane, and so such measurements can not distinguish $n = 0$ swirl from $n = 2, 4, ..$ swirl.

The response of the flow field to a small disturbance of increasing amplitude is not conventional. Very small disturbances, those for which εRe is small, give rise to a linear response everywhere. But this does not grow uniformly as ε is increased until a nonlinear description prevails. Instead, a domain of radius $O(\sqrt{\varepsilon})$ develops in the neighborhood of the center-line within which the response is $O(1)$, outside of which it remains small. Ultimately the response everywhere in the chamber becomes nonlinear because of the growth of this domain, the nonlinear patch.

Acknowledgement

This work was supported by AFOSR (JB, MS) and by the U.S. Department of Energy through the University of California under Subcontract number B341494 (JB, MS, SB).

REFERENCES

TAYLOR, G.I. 1956 Fluid flow in regions bounded by porous surfaces. *Proc. Roy. Soc. Lond A* **234**, 456-475.

CULICK, F.E.C. 1966 Rotational axisymmetric mean flow and damping of acoustic waves in solid propellant rocket motors. *AIAA J.* 4 1462-1464.

SUTTON, G. 1992 Rocket Propulsion Elements. Sixth Edition, John Wiley & Sons, NY. p.391.

DUNLAP, R., BLACKNER, A.M., WAUGH, R.C., BROWN, R.S., WILLOUGHBY, P.G. 1990 Internal flow field studies in a simulated cylindrical port rocket chamber. *J. Propulsion* **6** 690-704.

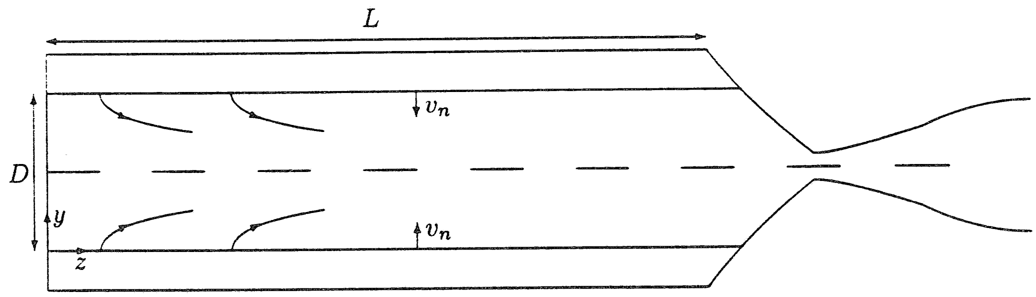

FIGURE 1. Rocket chamber Configuration

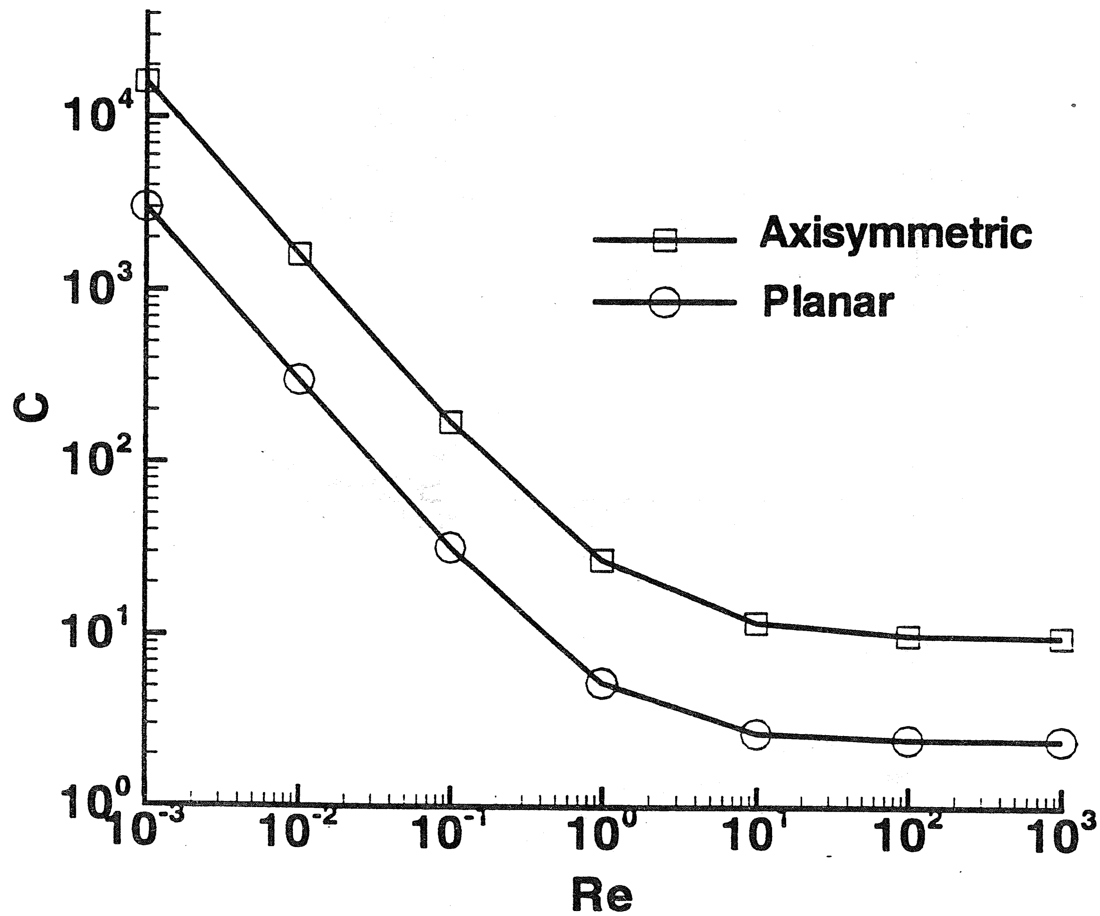

FIGURE 2. Variations of pressure gradient C with Reynolds Re for steady viscous solutions.

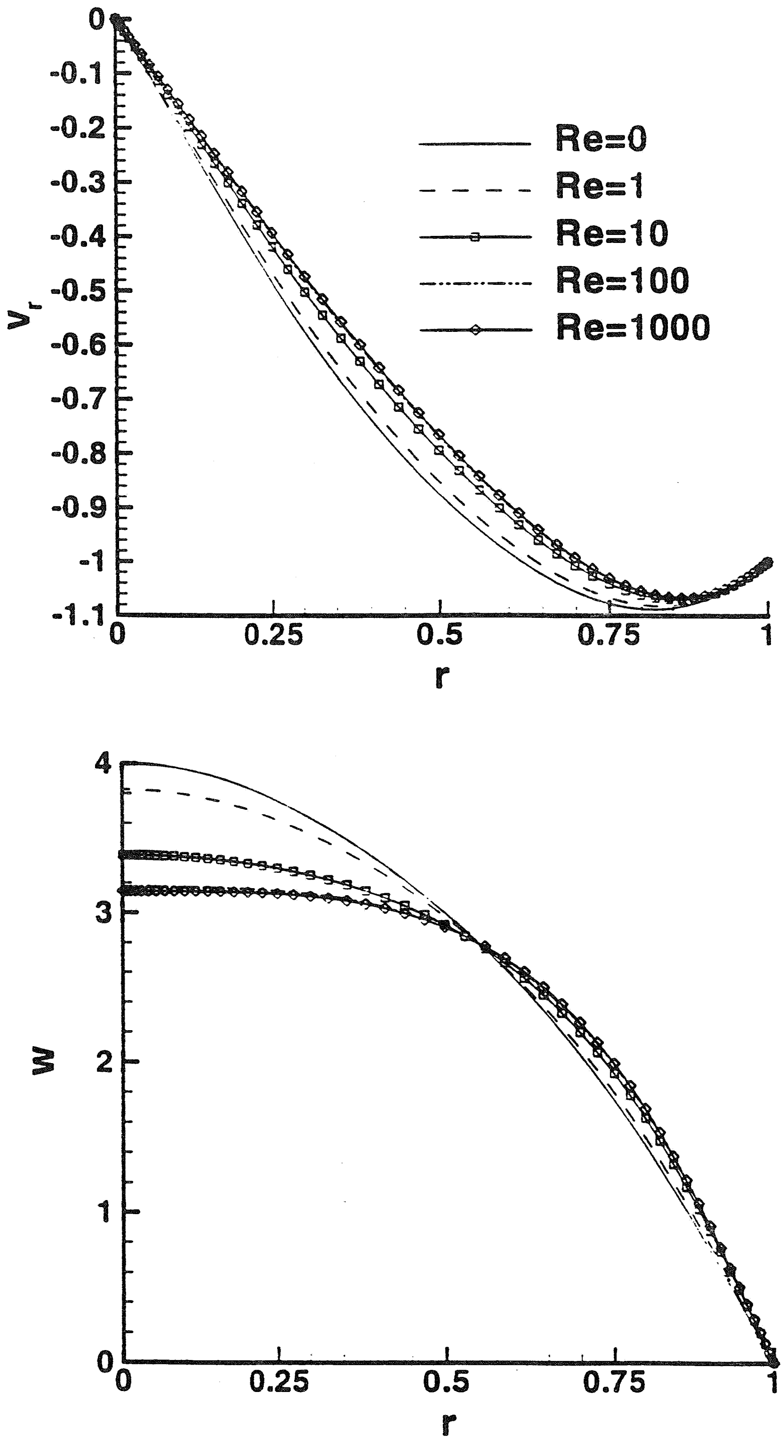

FIGURE 3. Axisymmetric viscous steady velocity field.

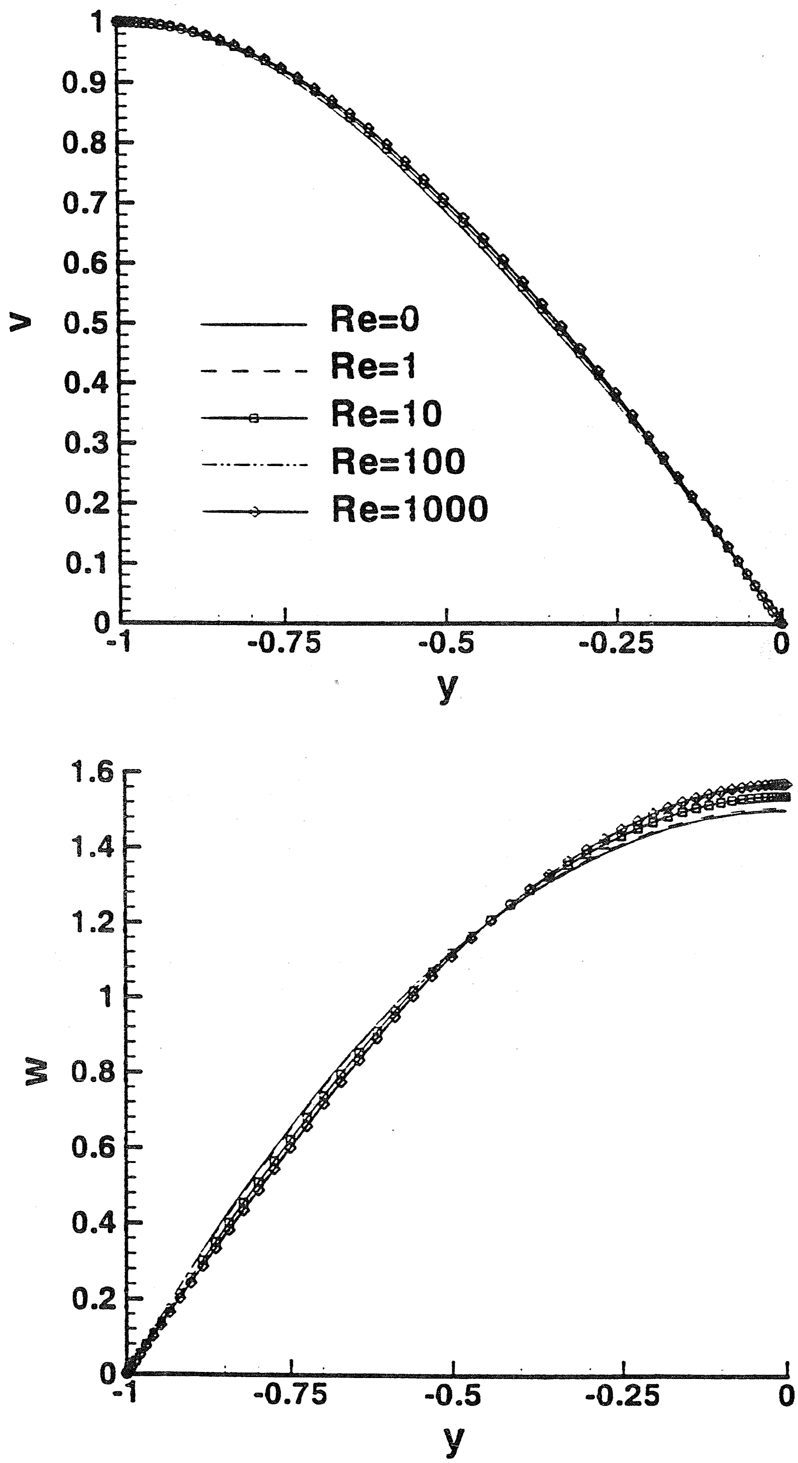

FIGURE 4. Plane viscous steady velocity field.

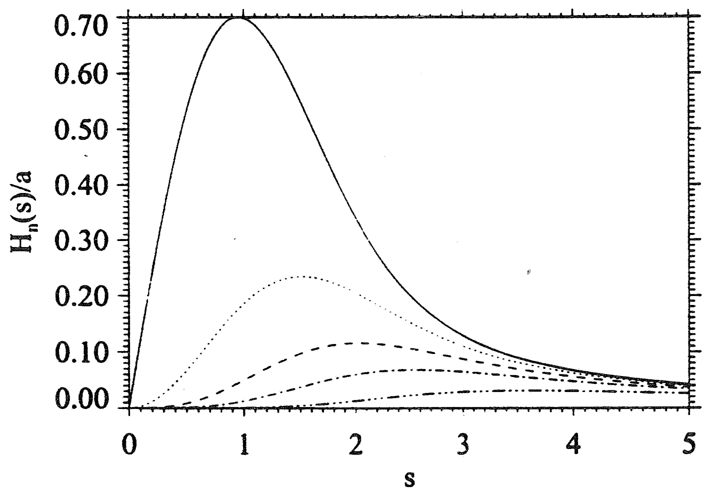

FIGURE 5. $H_n(s)/a$ against s for $n = 1$ (solid), $n = 2$ (dotted), $n = 3$ (dashed), $n = 4$ (dash-dot) and $n = 6$ (dash-dot-dot-dot).

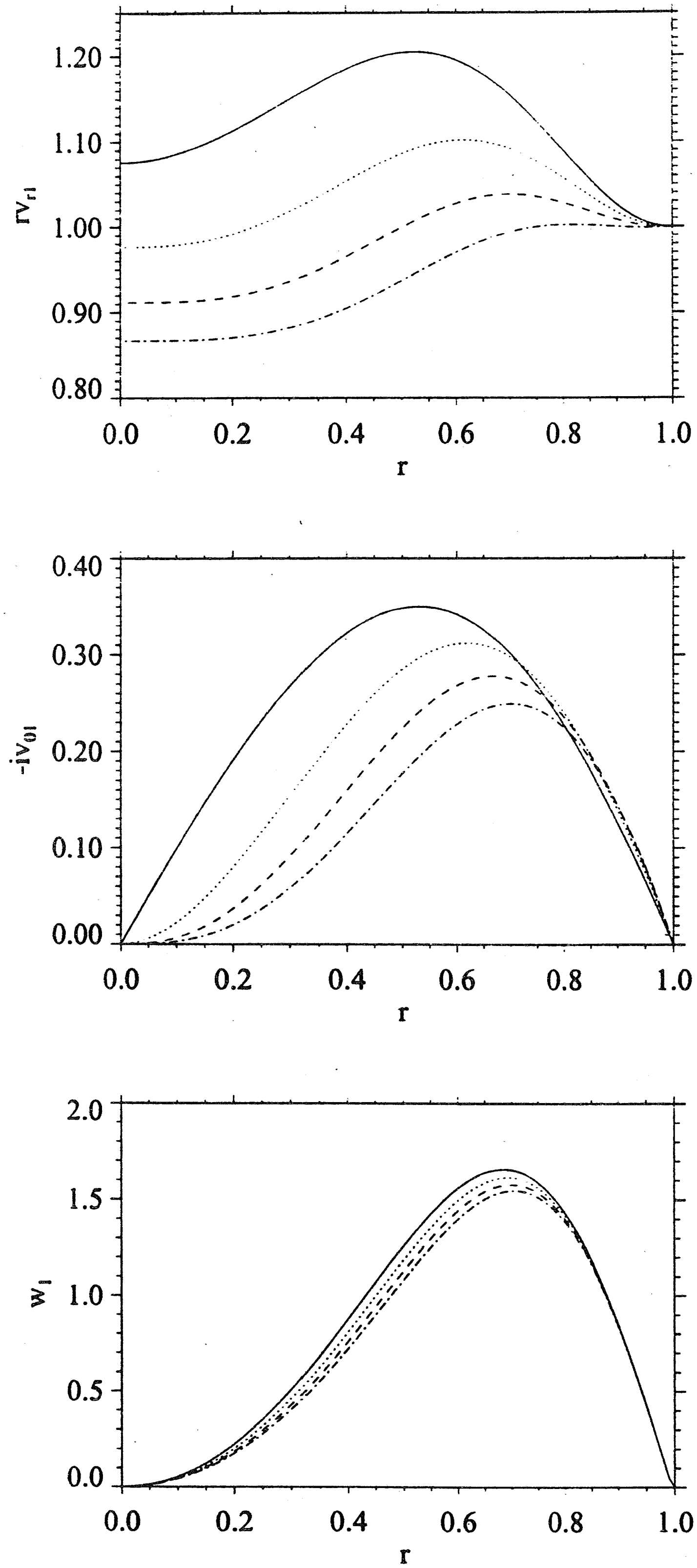

FIGURE 6. The behaviour of v_{r_1}, $-\mathrm{i}v_{\theta_1}$ and w_1 in the inviscid annulus for the perturbed velocity problem with the modes $n = 2$ (solid lines, $\bar{A} = 3.397$), $n = 3$ (dotted lines, $\bar{A} = 4.6016$), $n = 4$ (dashed lines. $\bar{A} = 5.7285$) and $n = 5$ (dot-dash lines, $\bar{A} = 6.8061$.) Here $A = \mathrm{i}\bar{A}$.

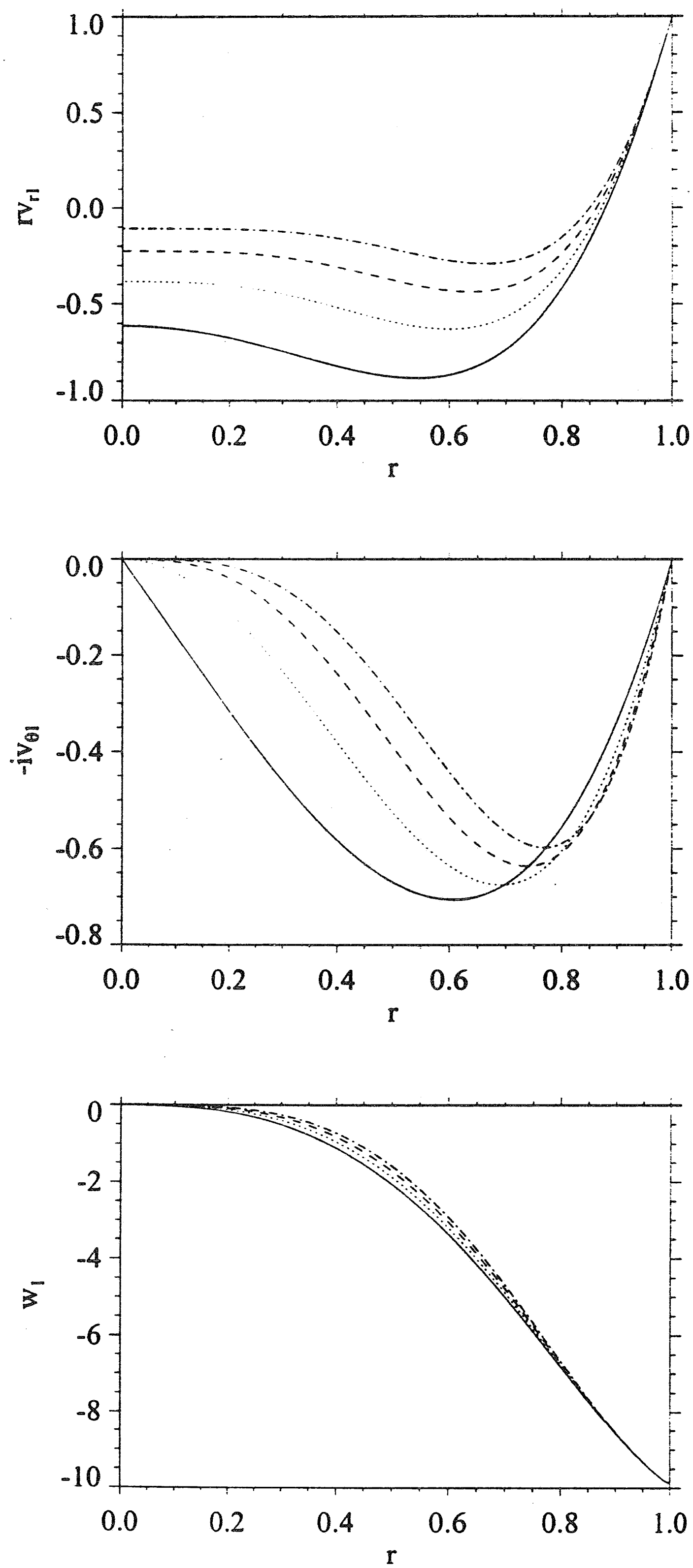

FIGURE 7. The behaviour of v_{r_1}, $-iv_{\theta_1}$ and w_1 in the inviscid annulus for the perturbed cylinder problem with the modes $n = 2$ (solid lines, $\bar{A} = -1.9245$), $n = 3$ (dotted lines, $\bar{A} = -1.8067$), $n = 4$ (dashed lines, $\bar{A} = -1.4102$) and $n = 5$ (dot-dash lines, $\bar{A} = -0.8467$.) Here $A = i\bar{A}$.

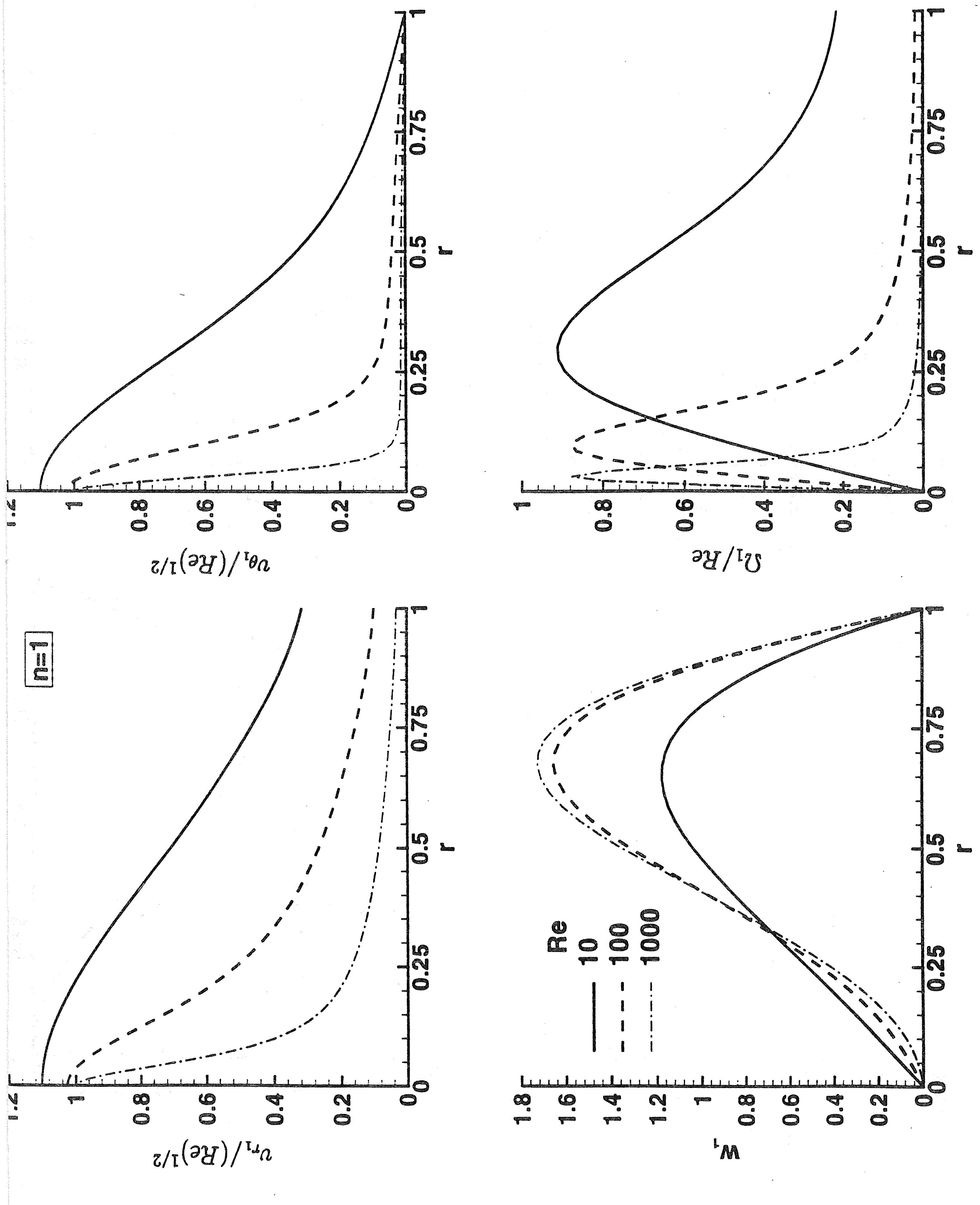

FIGURE 8. Perturbation solution when the injection velocity is perturbed, $n = 1$.

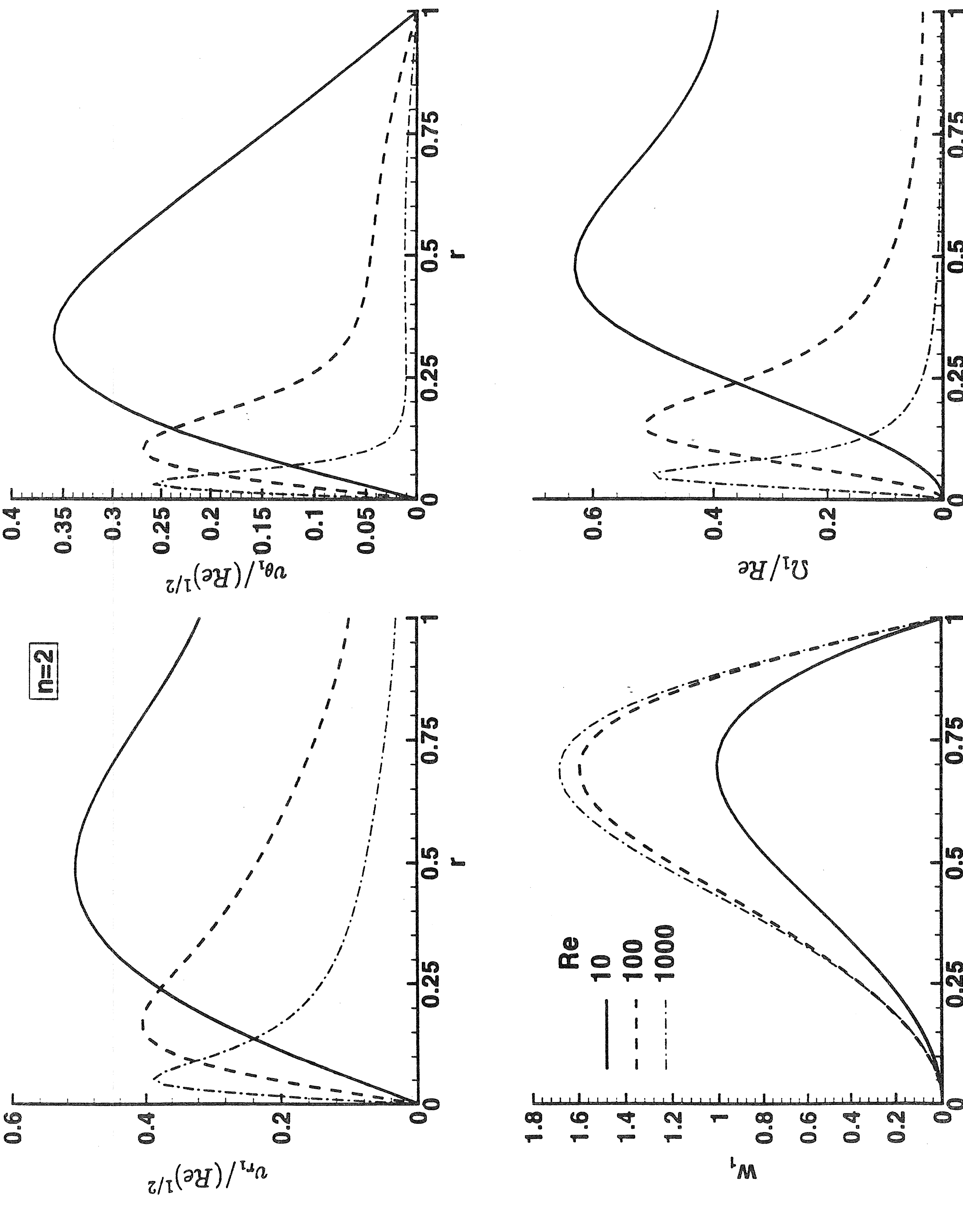

FIGURE 9. Perturbation solution when the injection velocity is perturbed, $n = 2$.

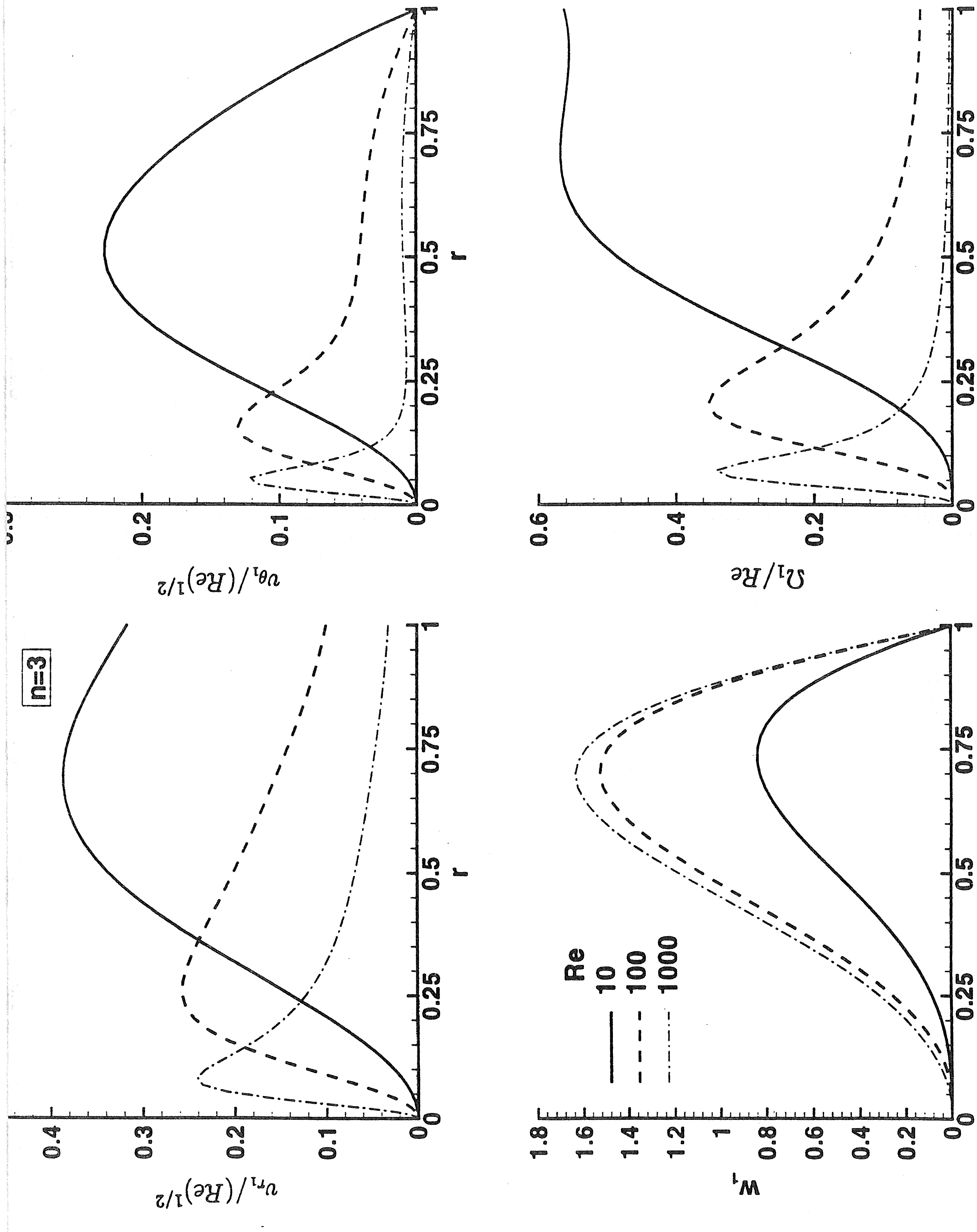

FIGURE 10. Perturbation solution when the injection velocity is perturbed $n = 3$.

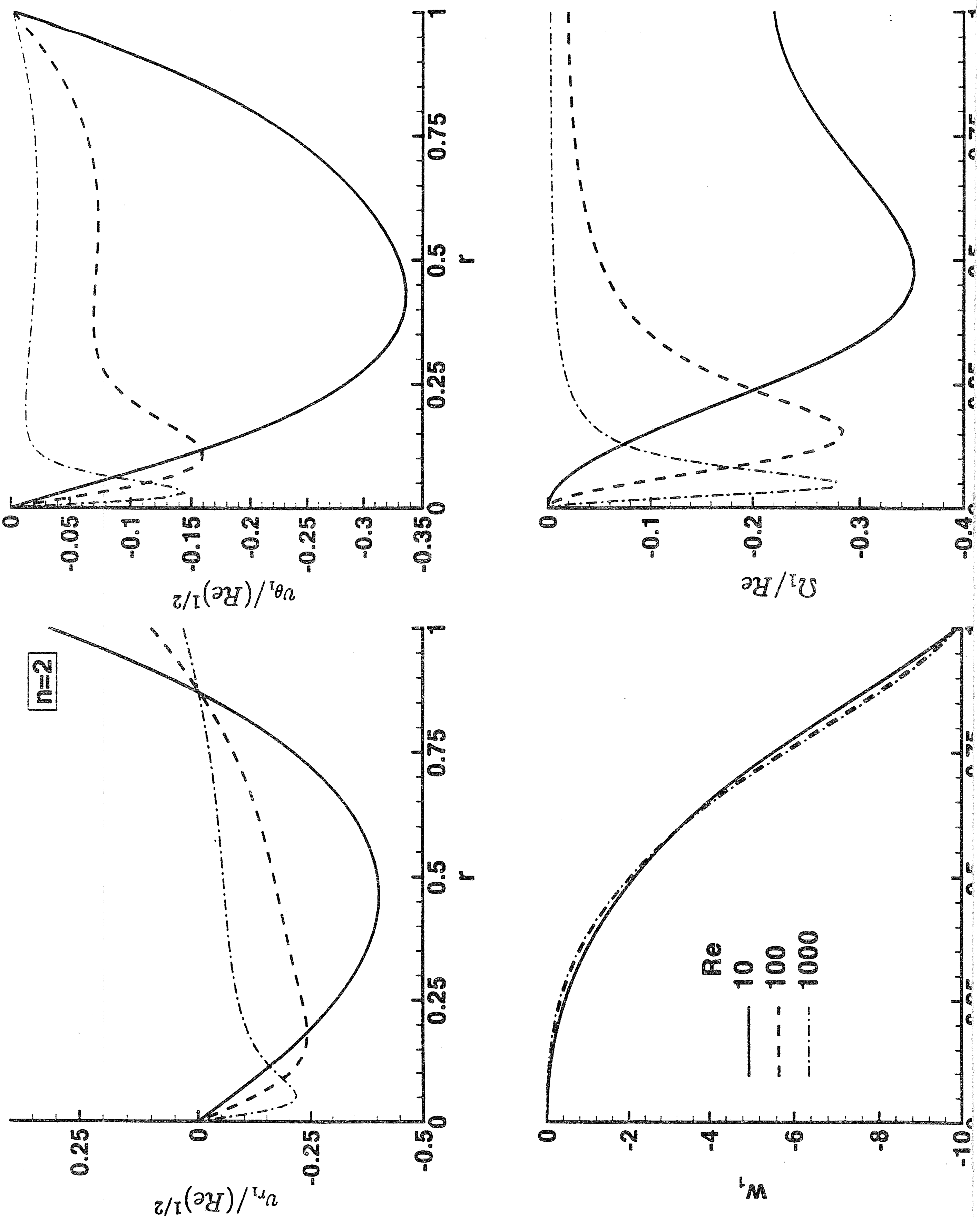

FIGURE 11. Perturbation solution when the radius is perturbed $n = 2$.

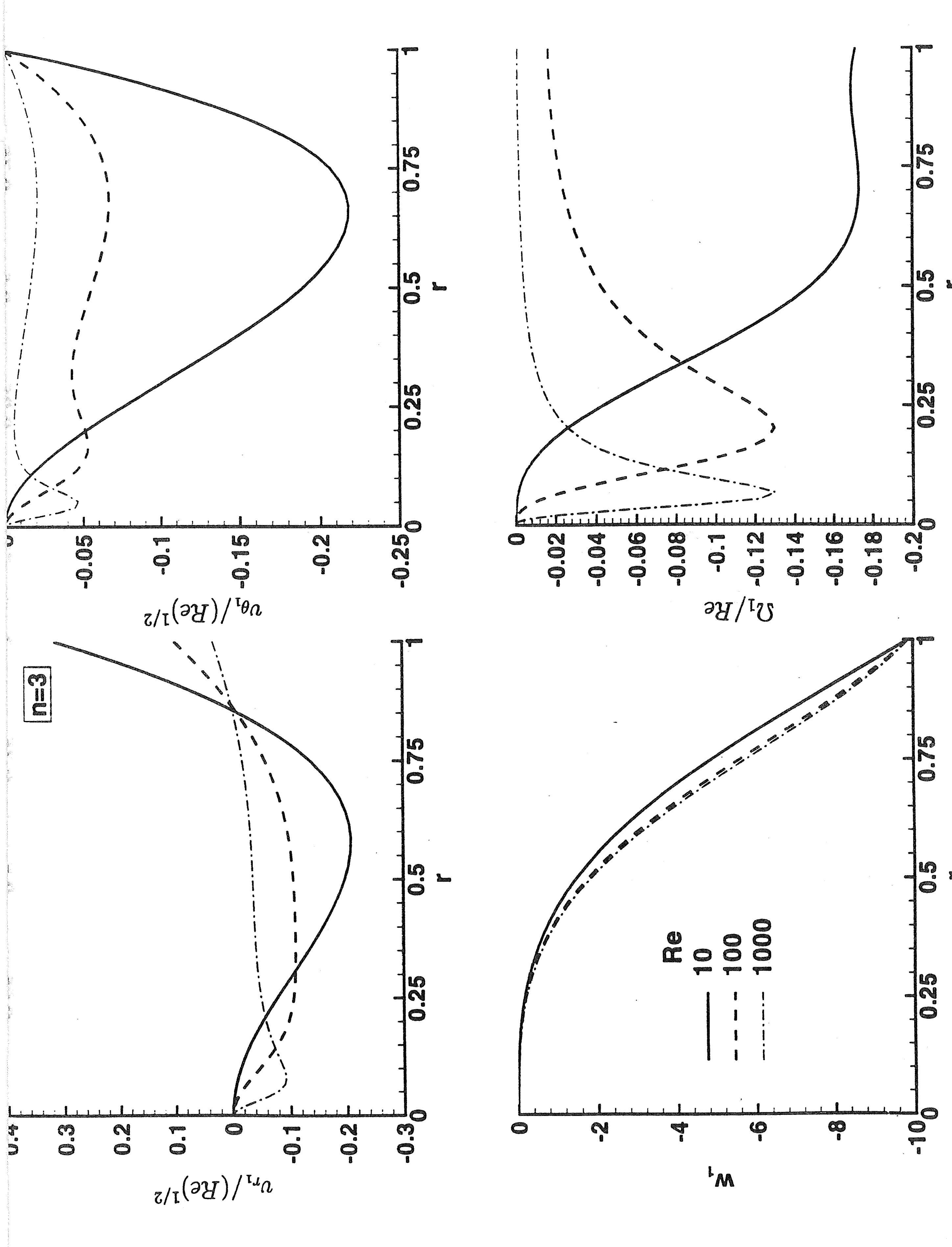

FIGURE 12. Perturbation solution when the radius is perturbed, $n = 3$.

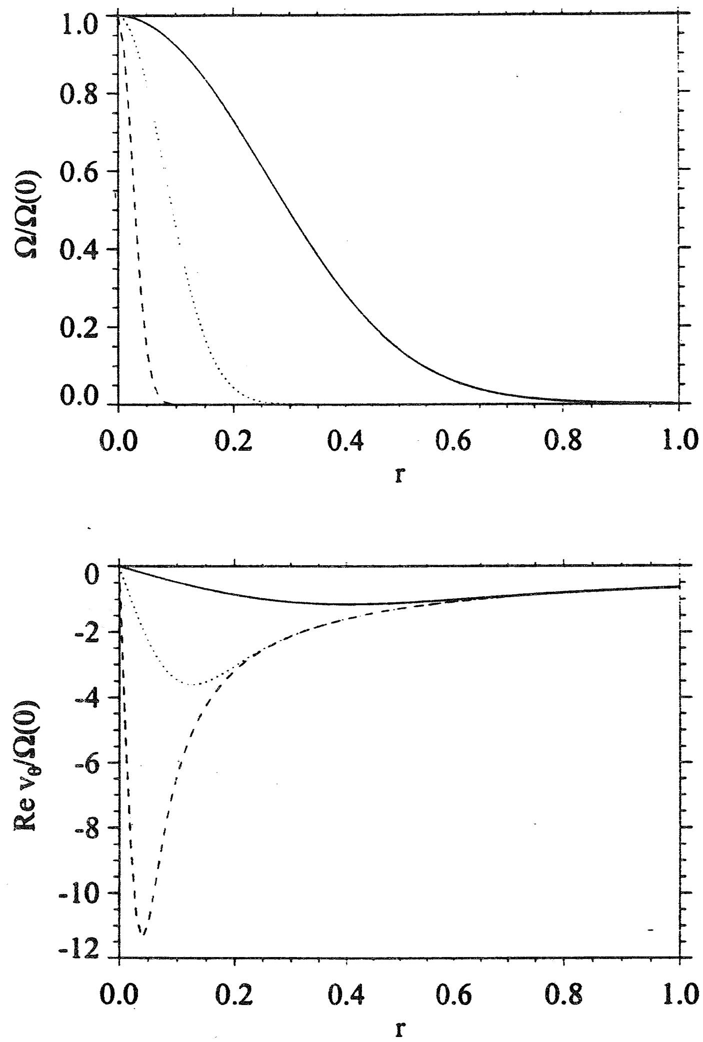

FIGURE 13. (a) Axial vorticity against r for Re = 10 (solid), Re = 100 (dotted) and Re = 1000 (dashed). $n = 0$. (b) Circumferential velocity against r for Re = 10 (solid), Re = 100 (dotted) and Re = 1000 (dashed), $n = 0$.

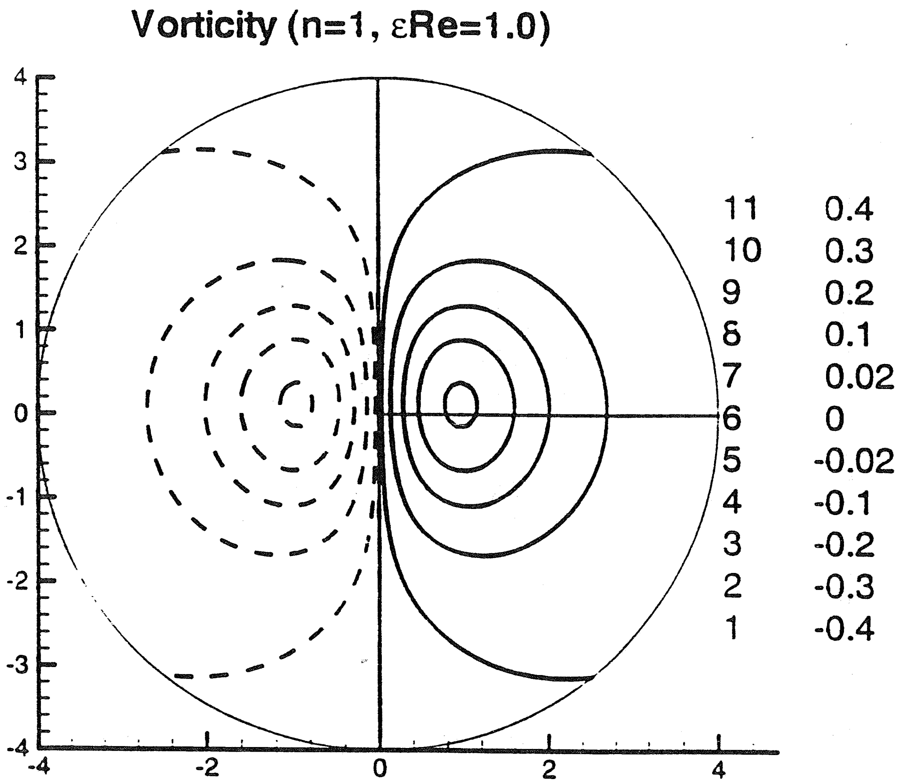
Vorticity (n=1, εRe=1.0)
4
3
2
1
0
-1
-2
-3
-4
-4
-2
0
2
4
11 0.4
10 0.3
9 0.2
8 0.1
7 0.02
6 0
5 -0.02
4 -0.1
3 -0.2
2 -0.3
1 -0.4

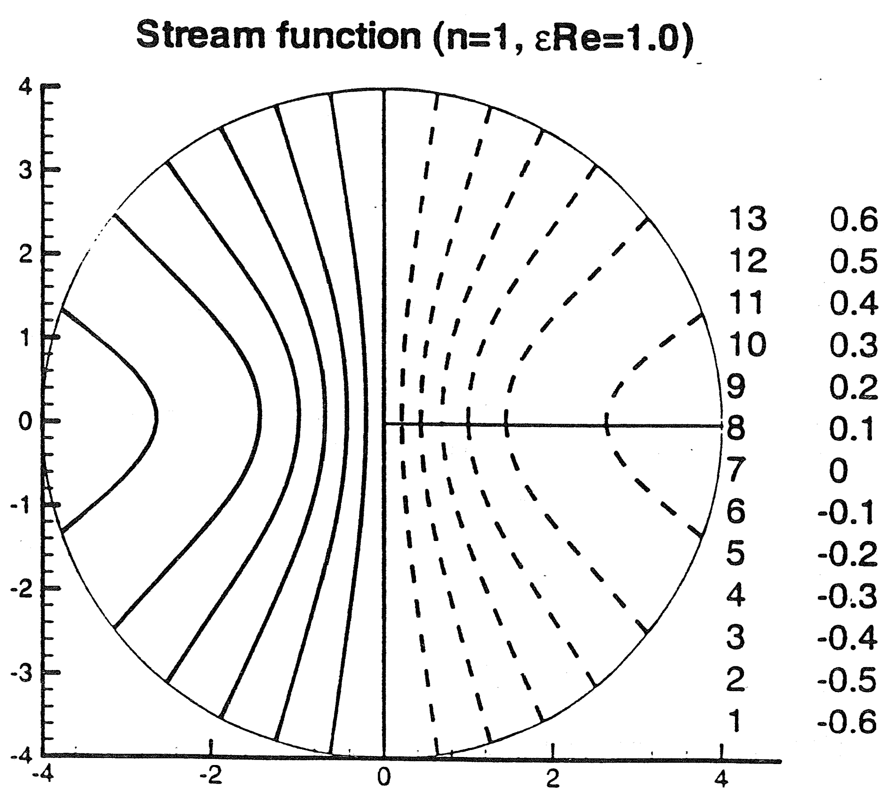
Stream function (n=1, εRe=1.0)
4
3
2
1
0
-1
-2
-3
-4
-4
-2
0
2
4
13 0.6
12 0.5
11 0.4
10 0.3
9 0.2
8 0.1
7 0
6 -0.1
5 -0.2
4 -0.3
3 -0.4
2 -0.5
1 -0.6

FIGURE 14.

Vorticity (n=1, εRe=10.0)

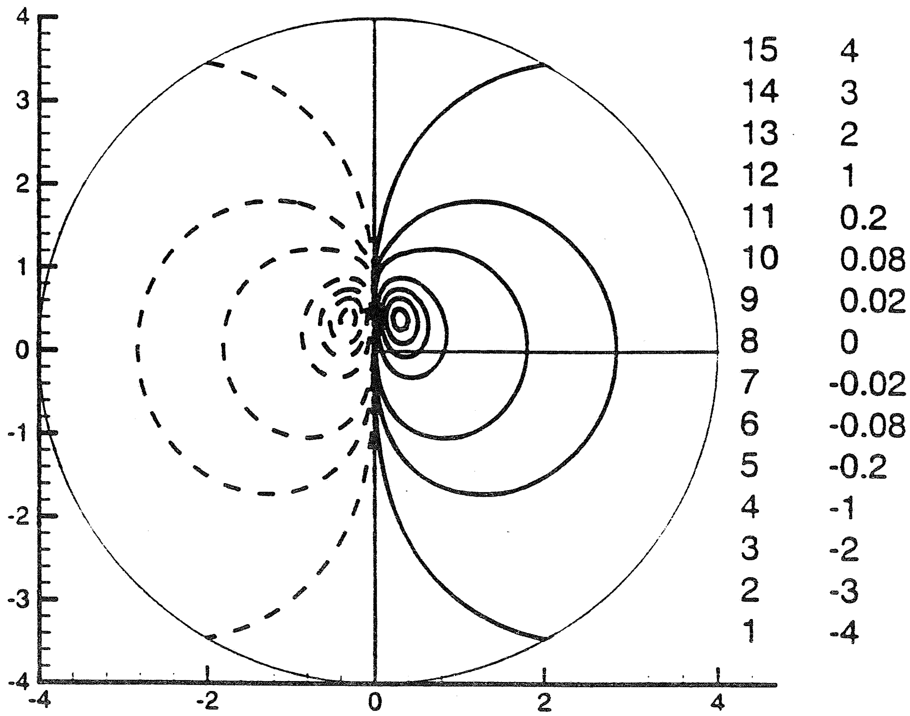

Stream function (n=1, εRe=10.0)

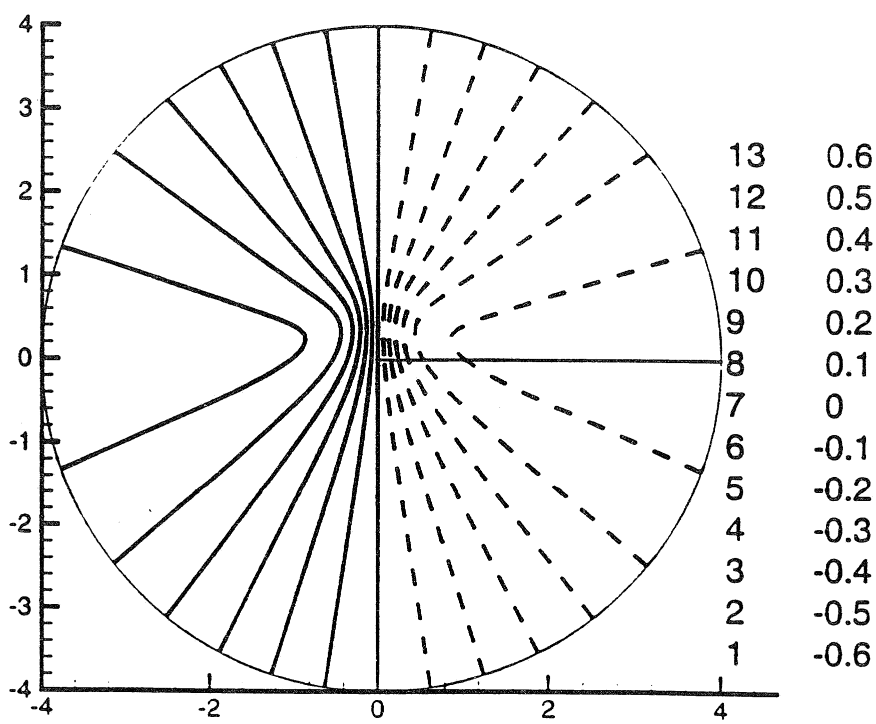

FIGURE 15.

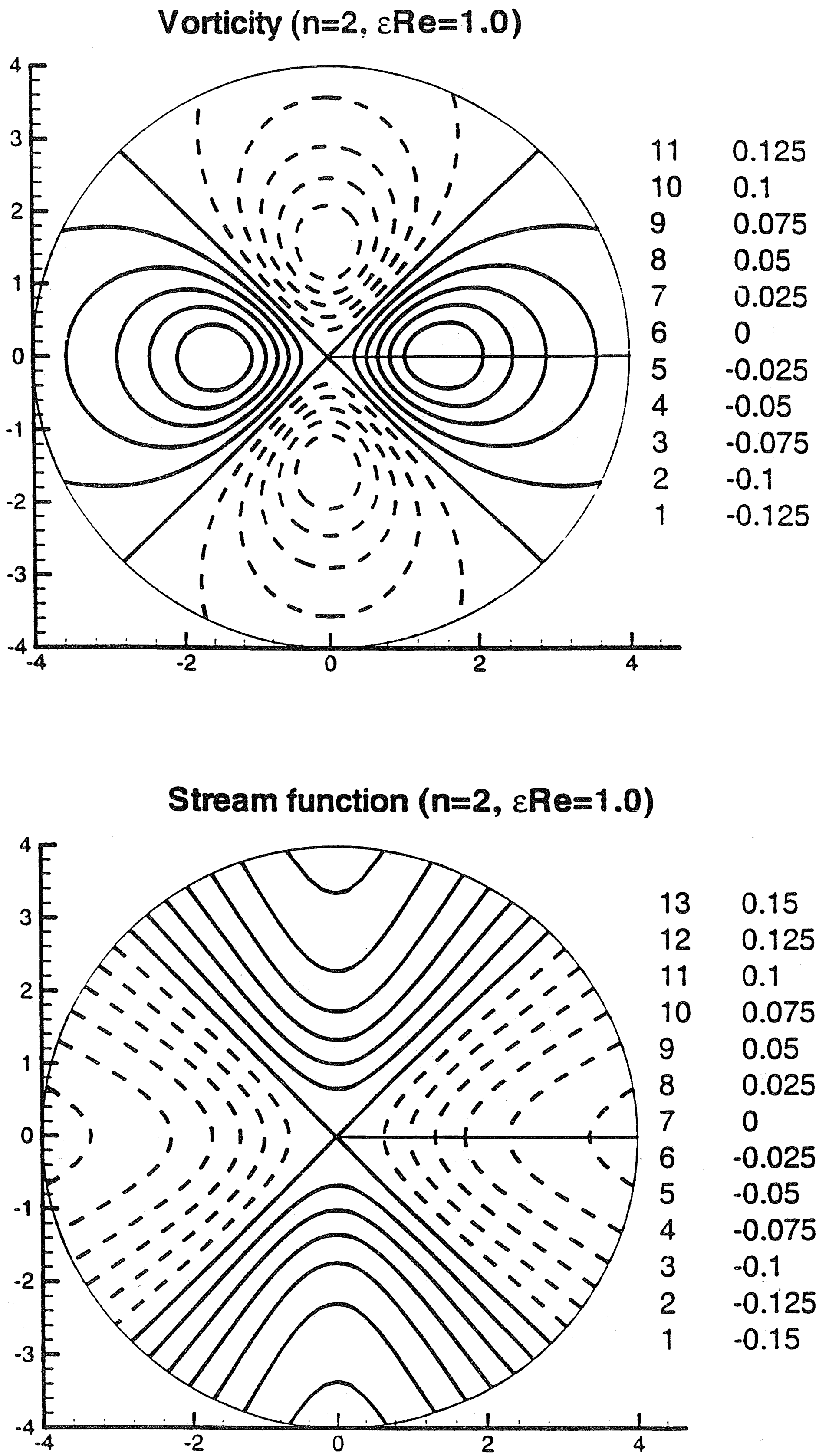
Vorticity (n=2, εRe=1.0)
4
3
2
1
0
-1
-2
-3
-4
-4
-2
0
2
4
11 0.125
10 0.1
9 0.075
8 0.05
7 0.025
6 0
5 -0.025
4 -0.05
3 -0.075
2 -0.1
1 -0.125
Stream function (n=2, εRe=1.0)
4
3
2
1
0
-1
-2
-3
-4
-4
-2
0
2
4
13 0.15
12 0.125
11 0.1
10 0.075
9 0.05
8 0.025
7 0
6 -0.025
5 -0.05
4 -0.075
3 -0.1
2 -0.125
1 -0.15

FIGURE 16.

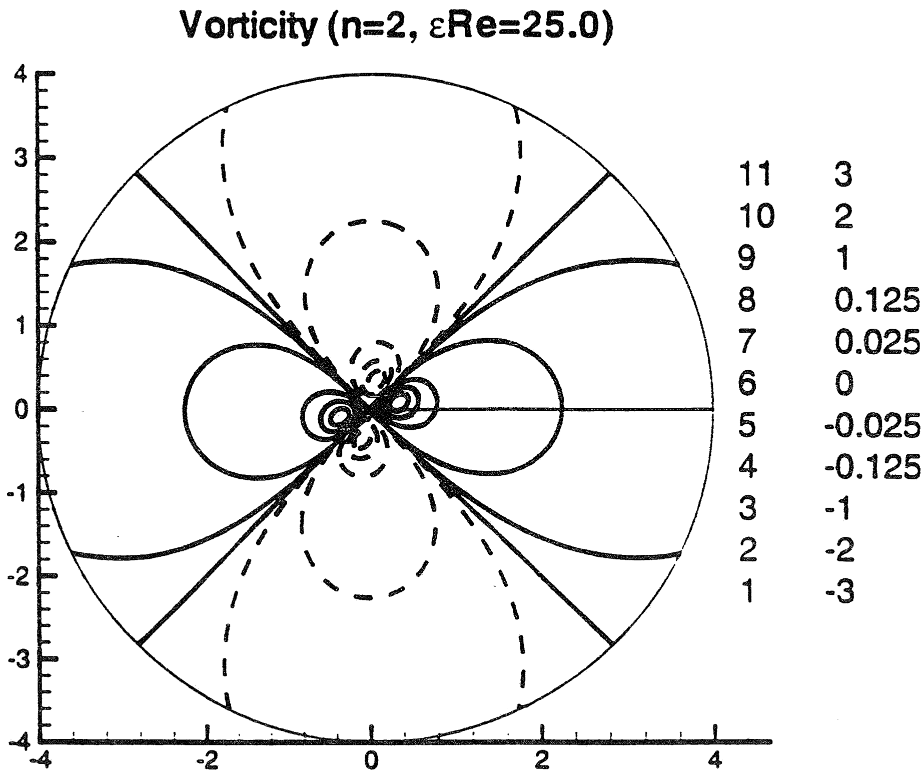
Vorticity (n=2, εRe=25.0)
4
3
2
1
0
-1
-2
-3
-4
-4
-2
0
2
4
11 3
10 2
9 1
8 0.125
7 0.025
6 0
5 -0.025
4 -0.125
3 -1
2 -2
1 -3

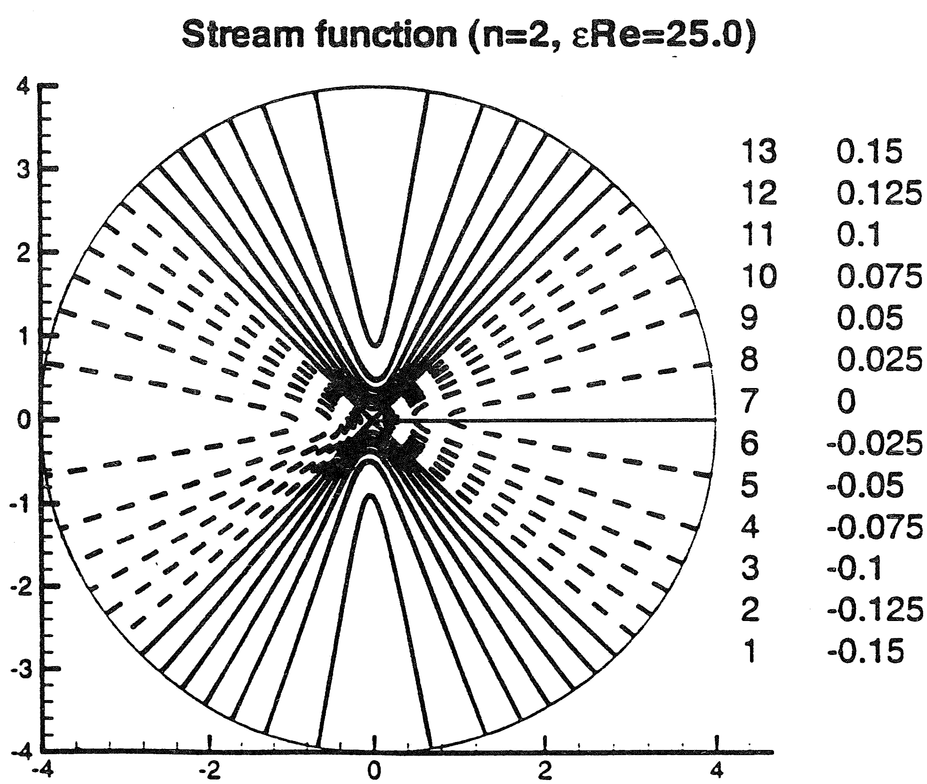
Stream function (n=2, εRe=25.0)
4
3
2
1
0
-1
-2
-3
-4
-4
-2
0
2
4
13 0.15
12 0.125
11 0.1
10 0.075
9 0.05
8 0.025
7 0
6 -0.025
5 -0.05
4 -0.075
3 -0.1
2 -0.125
1 -0.15

FIGURE 17.

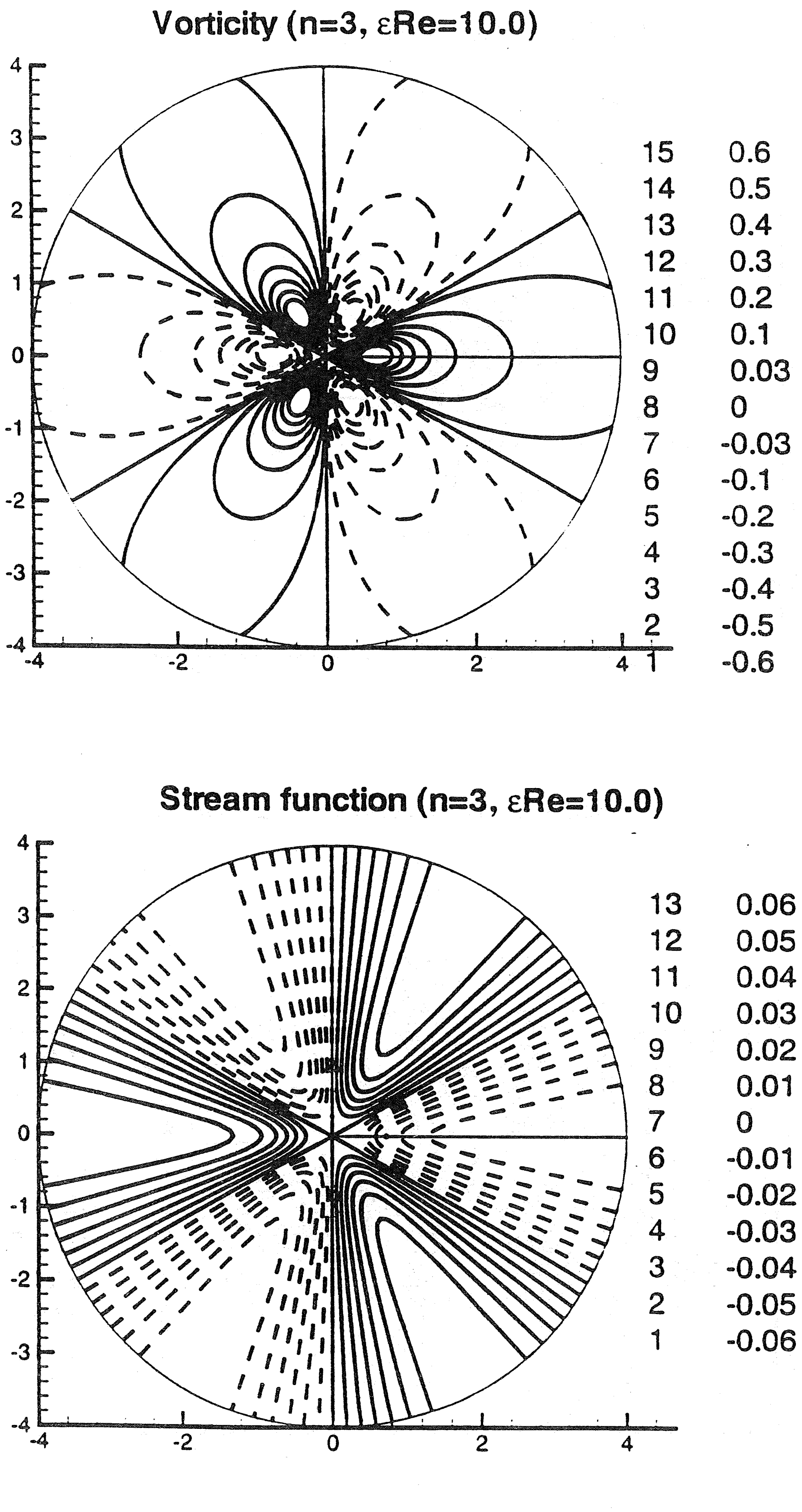
Vorticity (n=3, εRe=10.0)
4
3
2
1
0
-1
-2
-3
-4
-4
-2
0
2
4
15 0.6
14 0.5
13 0.4
12 0.3
11 0.2
10 0.1
9 0.03
8 0
7 -0.03
6 -0.1
5 -0.2
4 -0.3
3 -0.4
2 -0.5
1 -0.6
Stream function (n=3, εRe=10.0)
4
3
2
1
0
-1
-2
-3
-4
-4
-2
0
2
4
13 0.06
12 0.05
11 0.04
10 0.03
9 0.02
8 0.01
7 0
6 -0.01
5 -0.02
4 -0.03
3 -0.04
2 -0.05
1 -0.06

FIGURE 18.

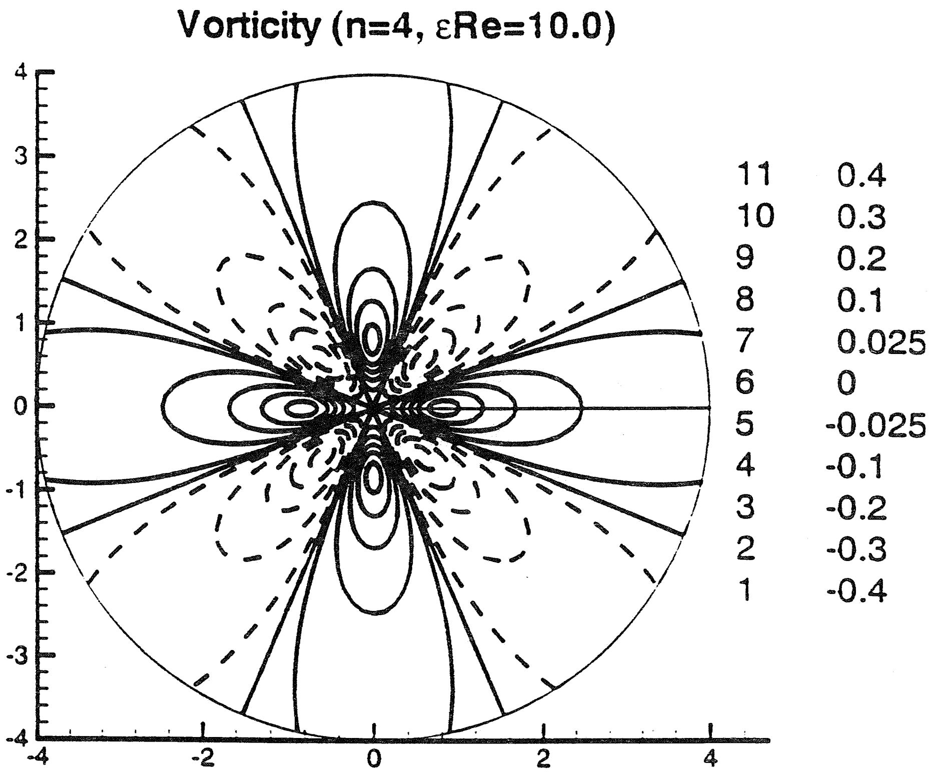
Vorticity (n=4, εRe=10.0)
11 0.4
10 0.3
9 0.2
8 0.1
7 0.025
6 0
5 -0.025
4 -0.1
3 -0.2
2 -0.3
1 -0.4

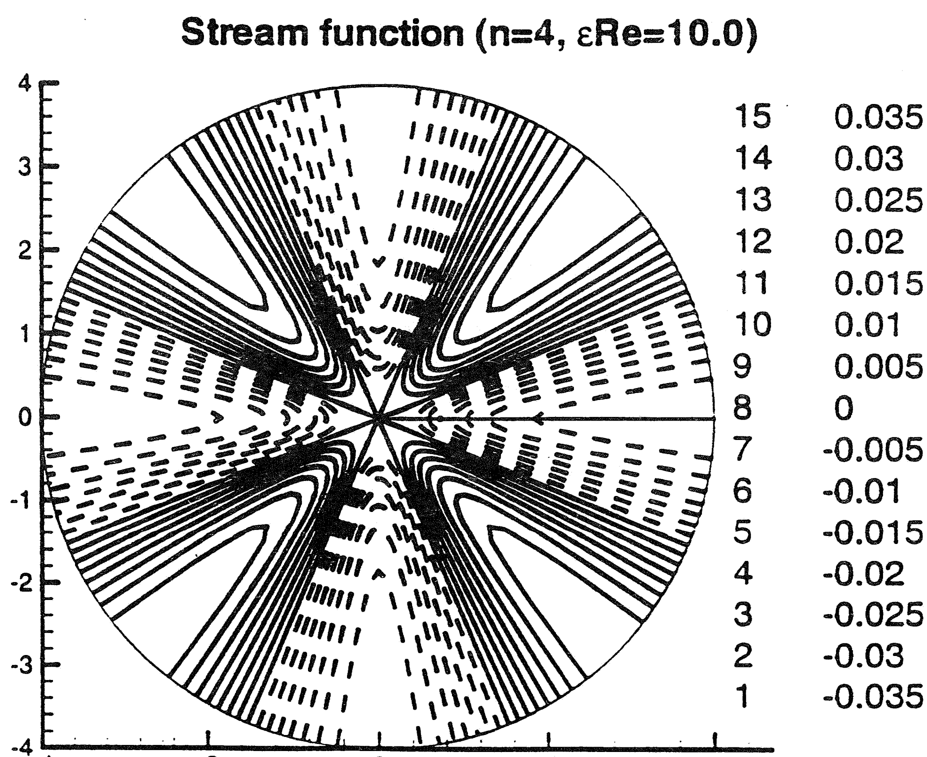
Stream function (n=4, εRe=10.0)
15 0.035
14 0.03
13 0.025
12 0.02
11 0.015
10 0.01
9 0.005
8 0
7 -0.005
6 -0.01
5 -0.015
4 -0.02
3 -0.025
2 -0.03
1 -0.035

FIGURE 19.

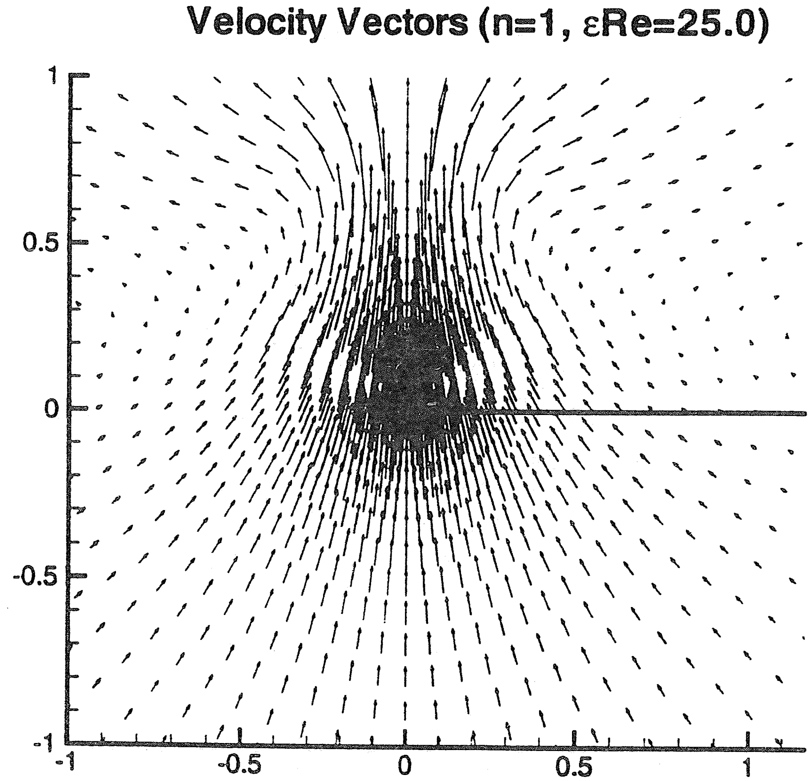
Velocity Vectors (n=1, εRe=25.0)
1
0.5
0
-0.5
-1
-1
-0.5
0
0.5
1

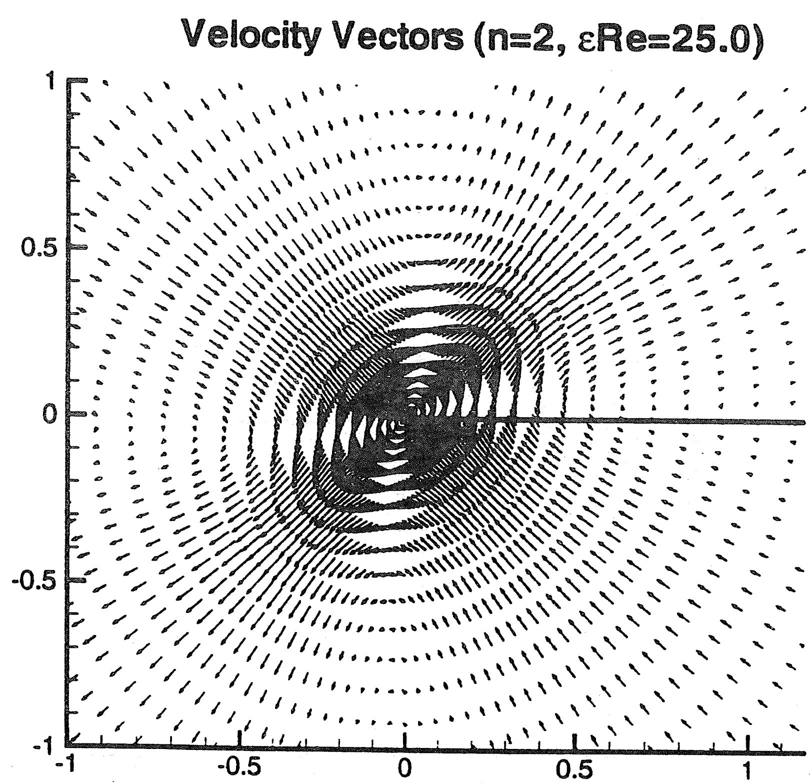
Velocity Vectors (n=2, εRe=25.0)
1
0.5
0
-0.5
-1
-1
-0.5
0
0.5
1

FIGURE 20. (a), (b)

Velocity Vectors (n=3, εRe=25.0)

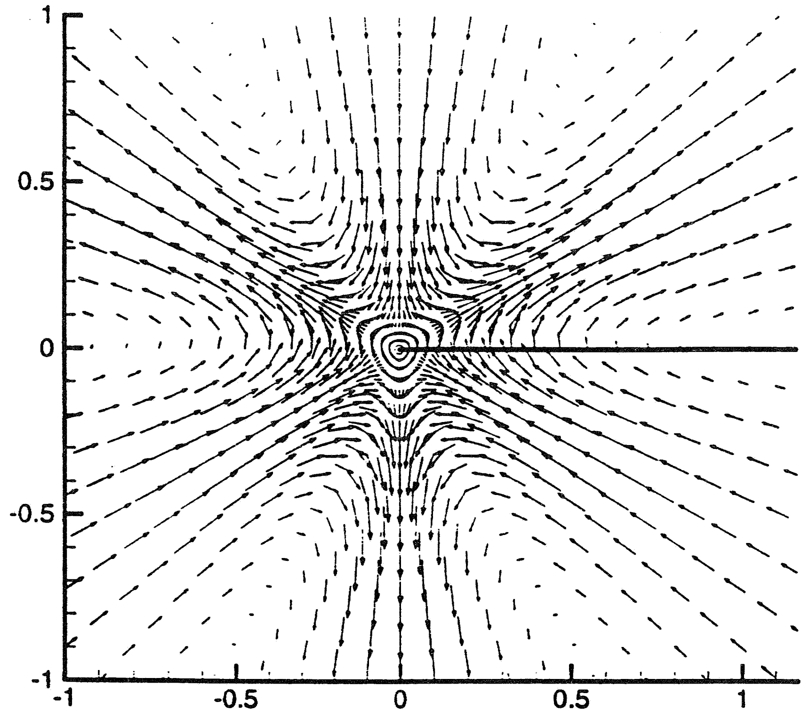

Velocity Vectors (n=4, εRe=25.0)

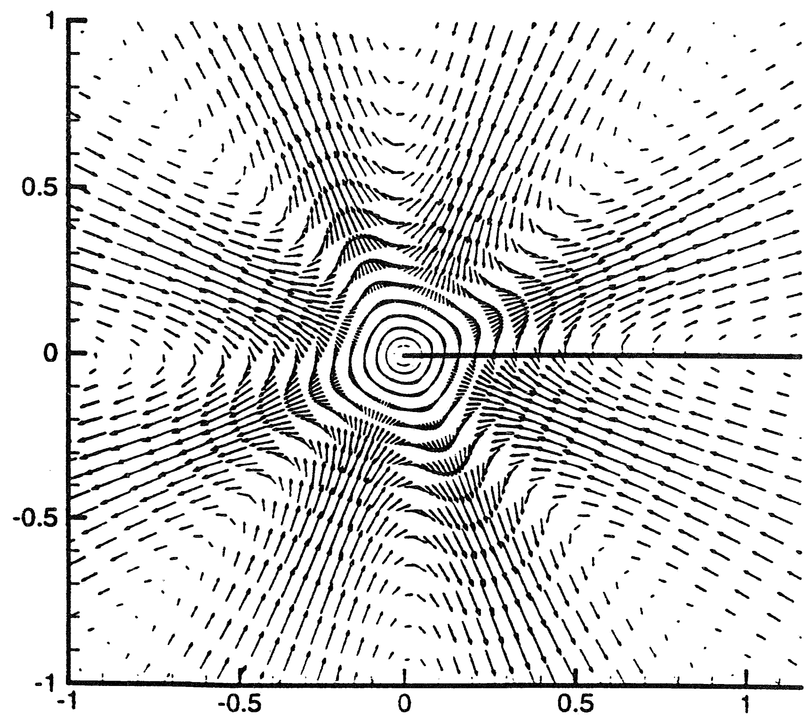

FIGURE 20. (c), (d)

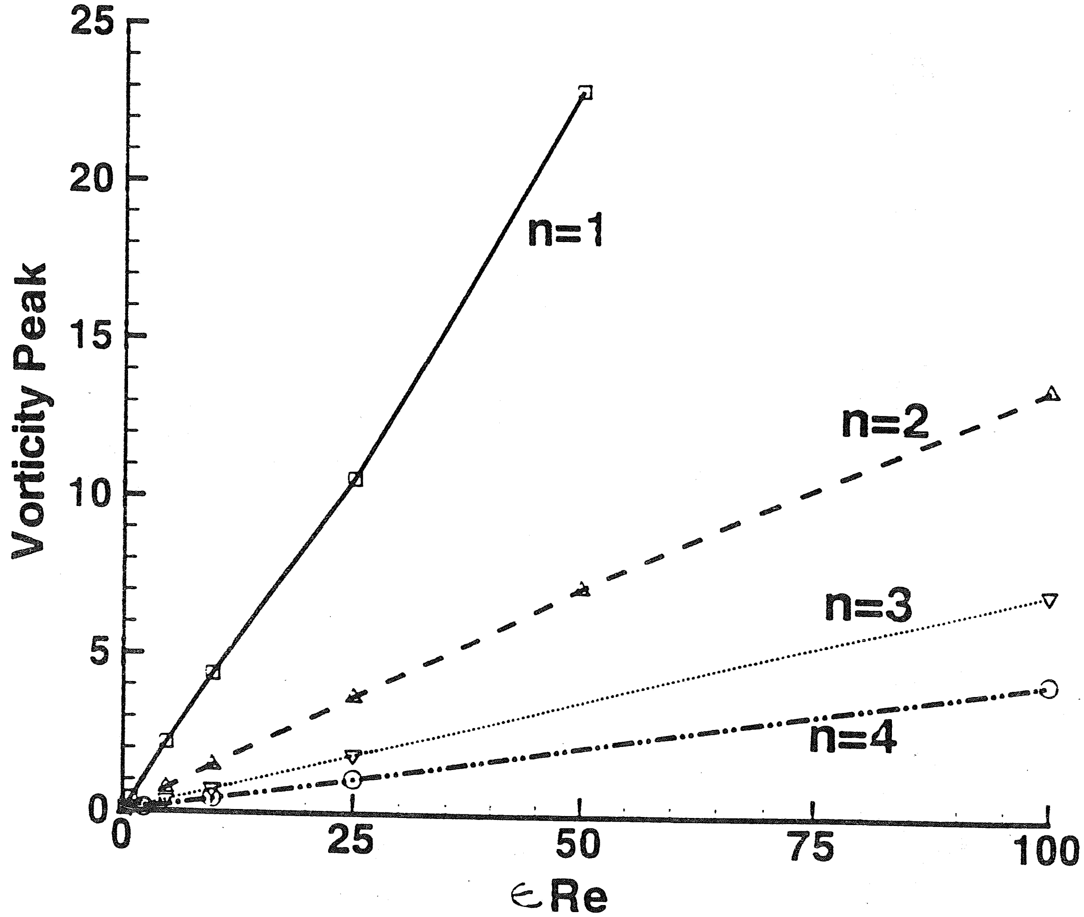

FIGURE 21.

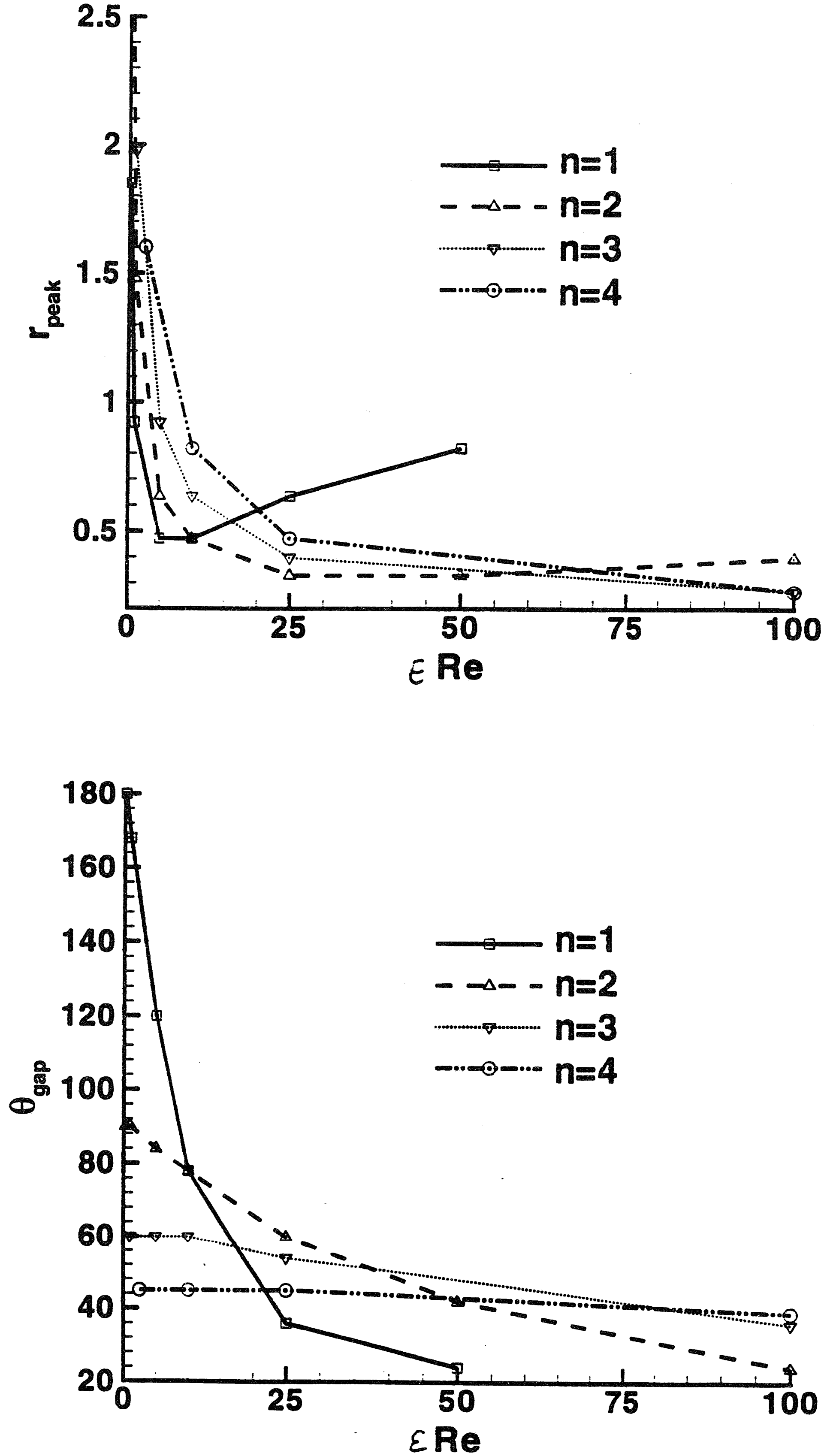
2.5
2
1.5
1
0.5
r_peak
n=1
n=2
n=3
n=4
0
25
50
75
100
ε Re
180
160
140
120
100
80
60
40
20
θ_gap
n=1
n=2
n=3
n=4
0
25
50
75
100
ε Re

FIGURE 22.

List of Recent TAM Reports

No.	Authors	Title	Date
815	Haber, R. B., C. S. Jog, and M. P. Bendsøe	A new approach to variable-topology shape design using a constraint on perimeter—*Structural Optimization* **11**, 1–12 (1996)	Feb. 1996
816	Xu, Z.-Q., and K. J. Hsia	A numerical solution of a surface crack under cyclic hydraulic pressure loading—*ASME Journal of Tribology* **119**, 637–645 (1997)	Mar. 1996
817	Adrian, R. J.	Bibliography of particle velocimetry using imaging methods: 1917–1995—*Produced and distributed in cooperation with TSI, Inc., St. Paul, Minn.*	Mar. 1996
818	Fried, E., and G. Grach	An order-parameter based theory as a regularization of a sharp-interface theory for solid–solid phase transitions—*Archive for Rational Mechanics and Analysis* **138**, 355–404 (1997)	Mar. 1996
819	Vonderwell, M. P., and D. N. Riahi	Resonant instability mode triads in the compressible boundary-layer flow over a swept wing—*International Journal of Engineering Science* **36**, 599–624 (1998)	Mar. 1996
820	Short, M., and D. S. Stewart	Low-frequency two-dimensional linear instability of plane detonation—*Journal of Fluid Mechanics* **340**, 249–295 (1997)	Mar. 1996
821	Casagranda, A., and P. Sofronis	On the scaling laws for the consolidation of nanocrystalline powder compacts—Proceedings of the *IUTAM Symposium on the Mechanics of Granular and Porous Materials*, N. A. Fleck and A. C. F. Cocks, eds. The Netherlands: Kluwer Academic Publishers, 105–116 (1997)	Apr. 1996
822	Xu, S., and D. S. Stewart	Deflagration-to-detonation transition in porous energetic materials: A comparative model study—*Journal of Engineering Mathematics* **31**, 143–172 (1997)	Apr. 1996
823	Weaver, R. L.	Mean and mean-square responses of a prototypical master/fuzzy structure—*Journal of the Acoustical Society of America* **101**, 1441–1449 (1997)	Apr. 1996
824	Fried, E.	Correspondence between a phase-field theory and a sharp-interface theory for crystal growth—*Continuum Mechanics and Thermodynamics* **9**, 33–60 (1997)	Apr. 1996
825	Students in TAM 293–294	Thirty-third student symposium on engineering mechanics, J. W. Phillips, coordinator: Selected senior projects by W. J. Fortino II, A. A. Mordock, and M. R. Sawicki	May 1996
826	Riahi, D. N.	Effects of roughness on nonlinear stationary vortices in rotating disk flows—*Mathematical and Computer Modeling* **25**, 71–82 (1997)	June 1996
827	Riahi, D. N.	Nonlinear instabilities of shear flows over rough walls, *Far East Journal of Applied Mathematics*, in press (1998)	June 1996
828	Weaver, R. L.	Multiple scattering theory for a plate with sprung masses, mean responses—*Journal of the Acoustical Society of America* **101**, 3466–3414 (1997)	July 1996
829	Moser, R. D., M. M. Rogers, and D. W. Ewing	Self-similarity of time-evolving plane wakes *Journal of Fluid Mechanics*, in press (1998)	July 1996
830	Lufrano, J. M., and P. Sofronis	Enhanced hydrogen concentrations ahead of rounded notches and cracks: Competition between plastic strain and hydrostatic stress—*Acta Metallurgica et Materialia*, in press (1998)	July 1996
831	Riahi, D. N.	Effects of surface corrugation on primary instability modes in wall-bounded shear flows	Aug. 1996
832	Bechel, V. T., and N. R. Sottos	Application of debond length measurements to examine the mechanics of fiber pushout	Aug. 1996
833	Riahi, D. N.	Effect of centrifugal and Coriolis forces on chimney convection during alloy solidification—*Journal of Crystal Growth* **179** , 287–296 (1997)	Sept. 1996
834	Cermelli, P., and E. Fried	The influence of inertia on configurational forces in a deformable solid—*Proceedings of the Royal Society of London A* **453**, 1915–1927 (1997)	Oct. 1996
835	Riahi, D. N.	On the stability of shear flows with combined temporal and spatial imperfections	Oct. 1996

List of Recent TAM Reports (cont'd)

No.	Authors	Title	Date
836	Carranza, F. L., B. Fang, and R. B. Haber	An adaptive space–time finite element model for oxidation-driven fracture, *Computer Methods in Applied Mechanics and Engineering*, in press (1997)	Nov. 1996
837	Carranza, F. L., B. Fang, and R. B. Haber	A moving cohesive interface model for fracture in creeping materials, *Computational Mechanics* **19**, 517–521 (1997)	Nov. 1996
838	Balachandar, S., R. Mittal, and F. M. Najjar	Properties of the mean wake recirculation region in two-dimensional bluff body wakes—*Journal of Fluid Mechanics*, in press (1997)	Dec. 1996
839	Ti, B. W., W. D. O'Brien, Jr., and J. G. Harris	Measurements of coupled Rayleigh wave propagation in an elastic plate—*Journal of the Acoustical Society of America* **102**, 1528–1531	Dec. 1996
840	Phillips, W. R. C.	On finite-amplitude rotational waves in viscous shear flows—*Studies in Applied Mathematics* **100**, in press (1998)	Jan. 1997
841	Riahi, D. N.	Direct resonance analysis and modeling for a turbulent boundary layer over a corrugated surface—*Acta Mechanica*, in press (1998)	Jan. 1997
842	Liu, Z.-C., R. J. Adrian, C. D. Meinhart, and W. Lai	Structure of a turbulent boundary layer using a stereoscopic, large format video-PIV—*Developments in Laser Techniques and Fluid Mechanics*, 259–273 (1997)	Jan. 1997
843	Fang, B., F. L. Carranza, and R. B. Haber	An adaptive discontinuous Galerkin method for viscoplastic analysis—*Computer Methods in Applied Mechanics and Engineering* **150**, 191–198 (1997)	Jan. 1997
844	Xu, S., T. D. Aslam, and D. S. Stewart	High-resolution numerical simulation of ideal and non-ideal compressible reacting flows with embedded internal boundaries—*Combustion Theory and Modeling* **1**, 113–142 (1997)	Jan. 1997
845	Zhou, J., C. D. Meinhart, S. Balachandar, and R. J. Adrian	Formation of coherent hairpin packets in wall turbulence—In *Self-Sustaining Mechanisms in Wall Turbulence*, R. L. Panton, ed. Southampton, UK: Computational Mechanics Publications, 109–134 (1997)	Feb. 1997
846	Lufrano, J. M., P. Sofronis, and H. K. Birnbaum	Elastoplastically accommodated hydride formation and embrittlement—*Journal of Mechanics and Physics of Solids*, in press (1998)	Feb. 1997
847	Keane, R. D., N. Fujisawa, and R. J. Adrian	Unsteady non-penetrative thermal convection from non-uniform surfaces—In *Geophysical and Astrophysical Convection*, R. Kerr, ed. (1997)	Feb. 1997
848	Aref, H., and M. Brøns	On stagnation points and streamline topology in vortex flows—*Journal of Fluid Mechanics* **370**, 1–27 (1998)	Mar. 1997
849	Asghar, S., T. Hayat, and J. G. Harris	Diffraction by a slit in an infinite porous barrier—*Wave Motion*, in press (1998)	Mar. 1997
850	Shawki, T. G., H. Aref, and J. W. Phillips	Mechanics on the Web—Proceedings of the International Conference on Engineering Education (Aug. 1997, Chicago)	Apr. 1997
851	Stewart, D. S., and J. Yao	The normal detonation shock velocity–curvature relationship for materials with non-ideal equation of state and multiple turning points—*Combustion and Flame*, in press (1998)	Apr. 1997
852	Fried, E., A. Q. Shen, and S. T. Thoroddsen	Wave patterns in a thin layer of sand within a rotating horizontal cylinder—*Physics of Fluids* **10**, 10–12 (1998)	Apr. 1997
853	Boyland, P. L., H. Aref, and M. A. Stremler	Topological fluid mechanics of stirring	Apr. 1997
854	Parker, S. J., and S. Balachandar	Viscous and inviscid instabilities of flow along a streamwise corner—*Theoretical and Computational Fluid Dynamics*, in press (1997)	May 1997
855	Soloff, S. M., R. J. Adrian, and Z.-C. Liu	Distortion compensation for generalized stereoscopic particle image velocimetry—*Measurement Science and Technology* **8**, 1–14 (1997)	May 1997
856	Zhou, Z., R. J. Adrian, S. Balachandar, and T. M. Kendall	Mechanisms for generating coherent packets of hairpin vortices in near-wall turbulence—*Journal of Fluid Mechanics*, in press (1997)	June 1997

List of Recent TAM Reports (cont'd)

No.	Authors	Title	Date
857	Neishtadt, A. I., D. L. Vainshtein, and A. A. Vasiliev	Chaotic advection in a cubic stokes flow—*Physica D* **111**, 227 (1997).	June 1997
858	Weaver, R. L.	Ultrasonics in an aluminum foam—*Ultrasonics*, in press (1997)	July 1997
859	Riahi, D. N.	High gravity convection in a mushy layer during alloy solidification—In *Nonlinear Instability, Chaos and Turbulence*, D. N. Riahi and L. Debnath, eds., in press (1998)	July 1997
860	Najjar, F. M., and S. Balachandar	Low-frequency unsteadiness in the wake of a normal plate, *Journal of Fluid Mechanics*, in press (1997)	Aug. 1997
861	Short, M.	A parabolic linear evolution equation for cellular detonation instability	Aug. 1997
862	Short, M., and D. S. Stewart	Cellular detonation stability—I: A normal-mode linear analysis	Sept. 1997
863	Carranza, F. L., and R. B. Haber	A numerical study of intergranular fracture and oxygen embrittlement in an elastic–viscoplastic solid—*Journal of the Mechanics and Physics of Solids*, in press (1997)	Oct. 1997
864	Sakakibara, J., and R. J. Adrian	Whole-field measurement of temperature in water using two-color laser-induced fluorescence	Oct. 1997
865	Riahi, D. N.	Effect of surface corrugation on convection in a three-dimensional finite box of fluid-saturated porous material	Oct. 1997
866	Baker, C. F., and D. N. Riahi	Three-dimensional flow instabilities during alloy solidification	Oct. 1997
867	Fried, E.	Introduction (only) to *The Physical and Mathematical Foundations of the Continuum Theory of Evolving Phase Interfaces* (book containing 14 seminal papers dedicated to Morton E. Gurtin), Berlin: Springer-Verlag, in press (1998)	Oct. 1997
868	Folguera, A., and J. G. Harris	Coupled Rayleigh surface waves in a slowly varying elastic waveguide	Oct. 1997
869	Stewart, D. S.	Detonation shock dynamics: Application for precision cutting of metal with detonation waves	Oct. 1997
870	Shrotriya, P., and N. R. Sottos	Creep and relaxation behavior of woven glass/epoxy substrates for multilayer circuit board applications	Nov. 1997
871	Riahi, D. N.	Boundary wave–vortex interaction in channel flow at high Reynolds numbers, *Fluid Dynamics Research*, in press (1998)	Nov. 1997
872	George, W. K., L. Castillo, and M. Wosnik	A theory for turbulent pipe and channel flows—paper presented at *Disquisitiones Mechanicae* (Urbana, Ill., October 1996)	Nov. 1997
873	Aslam, T. D., and D. S. Stewart	Detonation shock dynamics and comparisons with direct numerical simulation	Dec. 1997
874	Short, M., and A. K. Kapila	Blow-up in semilinear parabolic equations with weak diffusion	Dec. 1997
875	Riahi, D. N.	Analysis and modeling for a turbulent convective plume—*Mathematical and Computer Modeling* **28**, 57–63 (1998)	Jan. 1998
876	Stremler, M. A., and H. Aref	Motion of three point vortices in a periodic parallelogram—*Journal of Fluid Mechanics*, in press (1999)	Feb. 1998
877	Dey, N., K. J. Hsia, and D. F. Socie	On the stress dependence of high-temperature static fatigue life of ceramics	Feb. 1998
878	Brown, E. N., and N. R. Sottos	Thermoelastic properties of plain weave composites for multilayer circuit board applications	Feb. 1998
879	Riahi, D. N.	On the effect of a corrugated boundary on convective motion	Feb. 1998
880	Riahi, D. N.	On a turbulent boundary layer flow over a moving wavy wall	Mar. 1998
881	Riahi, D. N.	Vortex formation and stability analysis for shear flows over combined spatially and temporally structured walls	June 1998
882	Short, M., and D. S. Stewart	The multi-dimensional stability of weak heat release detonations	June 1998

List of Recent TAM Reports (cont'd)

No.	Authors	Title	Date
883	Fried, E., and M. E. Gurtin	Coherent solid-state phase transitions with atomic diffusion: A thermomechanical treatment—*Journal of Statistical Physics* (1998)	June 1998
884	Langford, J. A., and R. D. Moser	Optimal large-eddy simulation formulations for isotropic turbulence	July 1998
885	Riahi, D. N.	Boundary-layer theory of magnetohydrodynamic turbulent convection—*Proceedings of the Indian National Academy (Physical Science)*, in press (1998)	Aug. 1998
886	Riahi, D. N.	Nonlinear thermal instability in spherical shells—in *Nonlinear Instability, Chaos and Turbulence* **2**, in press (1998)	Aug. 1998
887	Riahi, D. N.	Effects of rotation on fully non-axisymmetric chimney convection during alloy solidification	Sept. 1998
888	Fried, E., and S. Sellers	The Debye theory of rotary diffusion	Sept. 1998
889	Short, M., A. K. Kapila, and J. J. Quirk	The hydrodynamic mechanisms of pulsating detonation wave instability	Sept. 1998
890	Stewart, D. S.	The shock dynamics of multidimensional condensed and gas phase detonations	Sept. 1998
891	Kim, K. C., and R. J. Adrian	Very large-scale motion in the outer layer	Oct. 1998
892	Fujisawa, N., and R. J. Adrian	Three-dimensional temperature measurement in turbulent thermal convection by extended range scanning liquid crystal thermometry	Oct. 1998
893	Shen, A. Q., E. Fried, and S. T. Thoroddsen	Is segregation-by-particle-type a generic mechanism underlying finger formation at fronts of flowing granular media?	Oct. 1998
894	Shen, A. Q.	Mathematical and analog modeling of lava dome growth	Oct. 1998
895	Buckmaster, J. D., and M. Short	Cellular instabilities, sub-limit structures, and edge-flames in premixed counterflows	Oct. 1998
896	Harris, J. G.	*Elastic waves*—Part of a book to be published by Cambridge University Press	Dec. 1998
897	Paris, A. J., and G. A. Costello	Cord composite cylindrical shells	Dec. 1998
898	Students in TAM 293–294	Thirty-fourth student symposium on engineering mechanics (May 1997), J. W. Phillips, coordinator: Selected senior projects by M. R. Bracki, A. K. Davis, J. A. (Myers) Hommema, and P. D. Pattillo	Dec. 1998
899	Taha, A., and P. Sofronis	A micromechanics approach to the study of hydrogen transport and embrittlement	Jan. 1999
900	Ferney, B. D., and K. J. Hsia	The influence of multiple slip systems on the brittle–ductile transition in silicon	Feb. 1999
901	Fried, E., and A. Q. Shen	Supplemental relations at a phase interface across which the velocity and temperature jump	Mar. 1999
902	Paris, A. J., and G. A. Costello	Cord composite cylindrical shells: Multiple layers of cords at various angles to the shell axis	April 1999
903	Ferney, B. D., M. R. DeVary, K. J. Hsia, and A. Needleman	Oscillatory crack growth in glass	April 1999
904	Fried, E., and S. Sellers	Microforces and the theory of solute transport	April 1999
905	Balachandar, S., J. D. Buckmaster, and M. Short	The generation of axial vorticity in solid-propellant rocket-motor flows	May 1999